Doctoral Dissertation (Shinshu University)

Analyses of spatial dynamics and photosynthesis in kudzu community by remote sensing

September 2021

Hiroki Iwamoto

Department of Bioscience and Food Production Science

Contents

Chapter 1

Introduction

Background

Ecological traits and management of kudzu community

Kudzu (*Pueraria lobata* (Willd.) Ohwi) originated in East Asia and is used as a source of starch (Kosaki and Ito 2018) and fiber (Kawamoto 2018). It has now been naturalized to other continents and has caused economic and ecological problems (Forseth and Innis 2004). The ecological traits of kudzu have been investigated from the viewpoints of invasive weed management, forage production, and prevention of soil erosion.

In the temperate climate of Japan, kudzu shoots start to emerge from overwintering stems or crown roots in April and grow until October. The growth rate of its leaf area is the highest in July and September and relatively low in August (Tsugawa and Kayama 1981a). The carbohydrates produced in above-ground components are transported from leaves to the stems and roots and are consumed through the emergence of shoots in the next season (Rashid *et al*. 2017). The rooted node is detached from the stubble in several years and forms a new ramet (Tsugawa and Kayama 1976). Tsugawa and Kayama (1989) observed kudzu growth and expansion by transplanting in several densities and showed that root dry weight increases under closer spacings, which contributes to dry matter accumulation in sparse populations at the early stage of invasion. In addition, kudzu produces seeds with a hard coat, which is tolerant to a variety of climatic and edaphic conditions (Susko and Mueller 1999). The dormancy of buried seeds is broken by scarification and burning (Susko and Mueller 1999, Fukuda 2014), which allows kudzu to emerge immediately after disturbance. The structure of the kudzu community reaches a steady state in 3 years and prevents the recruitment of other plants (Kameyama 1978).

Effective management methods for eradication and containment of kudzu have been examined in many countries, especially Japan and the United States, and include mowing and grazing (Bonsi *et al*. 1992) and mechanical methods to damage and remove aboveground organs. Herbicides can damage the whole plant chemically. Diseases (Weaver *et al*. 2016) and herbivore insects (Frye *et al*. 2007, 2012) have also been investigated for biological control. Digging out the crown roots is appropriate for

eradication (Nishino *et al.* 2019), but it is expensive. To prevent shoots' expansion, some construction methods for the physical obstruction of climbing stems have been developed (Tanaka and Yamaguchi 2016, Okazaki *et al*. 2018, Yamamoto *et al*. 2018). It is suggested that kudzu should be damaged in the summer in Japan for controlling its spread because carbohydrate concentration in storage organs is lowest in the summer (Rashid *et al*. 2017). Moreover, it has been shown that intense harvesting or grazing before the transportation of photosynthetic products to roots eliminates kudzu population (Miller and Edwards 1983). However, immense effort is required to mow or remove these weeds in the summer season. Therefore, it is important to identify the correct sequence of applying these methods and to explore the optimal timing according to the growth of kudzu.

Modeling for optimal weed management

Limited resources should be allocated appropriately for the effective management of invasive weeds, as described in previous studies on the simulation of kudzu population dynamics. The concept of "weed management" includes aims such as eradication, containment, and prevention of expansion. Zhang and Shea (2012, 2019), based on the experiment on the invasive thistle, claimed that optimal treatment of weeds depends on the goals of management. Efforts should be made to reduce the rate of spread and to protect assets after failure in eradication and containment at the early stages of invasion (Auld and Johnson 2014). These processes include local eradication and local containment within specific areas. Monitoring and modeling on a management scale should provide the practical knowledge for optimal asset allocation to prevent weed spread.

Previous studies on spatial plant ecology have attempted modeling and simulation of spatial dynamics of weeds. Models of long-distance seed dispersal have been proposed (e.g., Shigesada 1992, Katul *et al*. 2005, Komuro and Koike 2005). In regards to weed management, Osawa *et al*. (2016) defined "risk" as the product of the invasion probability and the area of potentially damaged crop and generated a 5 km grid-based risk map of bur cucumber (*Sicyos angulatus* L.) based on the simulation of invasion probability by cellular automata model. The 5 km grid-based risk map should be valuable for eradication during the early stages of invasion but a risk map should be generated at a smaller scale for prevention of spread in the later stages.

Simulation models of kudzu's spatial dynamics have been proposed for the

optimization of management planning. Hughes *et al.* (2014) and Hoffberg *et al.* (2018) constructed grid-based growth models for simulation of kudzu control and demonstrated that optimal management strategies should depend on goals. Aurambout and Endress (2018) presented a model to simulate the population dynamics of kudzu on a real landscape. These precedents gave us general knowledge for kudzu management; however, they were virtual and did not refer to real observation data. The model based on spatially and temporally high-resolution monitoring data of real communities should be constructed to simulate kudzu community dynamics on a management scale. Spatially continuous and temporally sequential data with high resolution, such as unmanned aerial vehicle (UAV) imagery, should help interpret ecological traits and simulate kudzu's expansion.

Sensing of spatial data

Remote sensing provides us with the spectral reflectance of plant canopy as surface data. Destructive methods such as sampling in the field demand extensive labor to acquire surface data and cannot obtain time-series data of a community. Moreover, the imagery obtained by satellites or airplanes covers a wide range in a single observation without having to visit the site; however, its resolution is not enough to detect weed community and the timing of imaging can hardly be adjusted. In contrast, although remote sensing by UAV requires visiting the site to observe a relatively narrow range, the data is spatially continuous and of high resolution. In addition, it is easy to adjust the timing and the intervals of image obtainment according to the target and management goal. Therefore, monitoring with UAV imagery is suitable to evaluate weed community dynamics, as well as the effect of management.

A high-resolution aerial image facilitates extracting information of a particular species but the volume of data is too massive to classify the whole image manually. The installation of efficient programs is needed to extract information effectively and objectively. For the classification of plants in the image, the algorithm should be constructed flexibly to suit the target and situation (e.g., Suzuki *et al*. 2010, Louargant *et al*. 2017). The pixels on images must contain some noise; thus, object-based analysis has been adopted to classify vegetation (Lopez-Granados *et al*. 2016, Chabot *et al*. 2018). However, object-based detection is not suitable for time-series monitoring because the arrangement of objects differs depending on the timing of image acquisition. To evaluate

the temporal transition of vegetation, the presence/absence of each species should be judged in each fixed grid. Supervised learning should enable the construction of flexible classification models. It requires the results from the manual classification of a part of the image as training data but is appropriate to build an estimation model based on multiple attributes. Classification of plants from aerial images has been proposed and achieved high accuracy and replicability in the detection of the target plant (e.g., Oguma *et al.* 2016, Alexandridis *et al*. 2017).

In addition, the growth state of a community can be assessed spatially based on spectral reflectance obtained by UAV. Vegetation indices (VI) are calculated from the reflectance of multiple bands and mitigate the fluctuation of radiation and interference by structural features. The techniques to estimate leaf area index (LAI), biomass, and chlorophyll content from spectral reflectance have been applied mainly to crops and pastures for optimization of management (e.g., Inoue *et al.* 2008, Kawamura and Akiyama 2012). Watanabe *et al.* (2005) estimated the vegetation biomass on paddy levees using spectral reflectance measured by an airplane. However, the application of remote sensing to the weed community has not been used much before.

Most previous studies in remote sensing and machine learning for vegetation have been used as an alternative to conventional methods for vegetation monitoring and have focused on the techniques and accuracy. However, temporally and spatially high-resolution surface data provides us with qualitatively different information and knowledge on ecological traits, community dynamics, and optimal management of weeds. Sequential UAV images and detection of target weeds by imagery classification are useful to evaluate the expansion rate of a community's margin. For evaluation of spatial dynamics, it is appropriate to estimate LAI based on the result of species' classification because a weed community has many species and it is hard to target a single species. The kudzu community can be detected relatively easily on UAV imagery by machine learning because it has large leaves and covers other plants. Therefore, UAV imagery is suitable to evaluate the spatial distribution and dynamics of the kudzu community.

Sensing of physiological function

Efficient photosynthesis in the summer is essential for the accumulation of carbohydrates into the storage organs of kudzu. However, the photosynthetic function of kudzu does not seem to be suitable in the summer as the photosynthetic rate of kudzu is

saturated at 1000 μmol photons m^{-2} s^{-1} and decreases at a temperature of more than 30 ℃ (Sharkey and Loreto 1993). Kudzu has been known for the diurnal movement of its leaves since ancient times in Japan and was called “urami-gusa” (the plant that shows the back of the leaves) for this behavior. Forseth and Teramura (1986) reported kudzu’s leaf orientation for the first time academically and demonstrated that it reduced midday irradiance, leaf temperature, and transpirational water loss. The movement includes diaheliotropism in the morning and dusk and paraheliotropism in midday (Liu *et al*. 1997a) and contributes to the maintenance of photosynthetic rate by regulating leaf temperature and preventing water loss (Liu *et al*. 1997b). This behavior seems to affect the light interception and photosynthetic efficiency of a whole canopy but has not been investigated yet.

It is technically challenging to measure photosynthetic function in the field. This is because parameters of photosynthetic function are measured in a short time as photosynthetic activity is sensitive to light conditions rapidly changing inside the canopy. It is not practical to measure CO_2 absorption directly in a short time, but chlorophyll fluorescence can be measured rapidly by pulse amplitude modulation (PAM) fluorometry. PAM is widely utilized to evaluate photosynthetic functions under various environmental and physiological conditions. A portable device has been developed (Kuhlgert *et al*. 2016) and is suitable for monitoring the photosynthetic activity of a plant or canopy. This should enable the examination of physiological function plasticity and survival strategy of weeds.

Purpose

In this study, I evaluated the ecological traits and optimal management of kudzu with novel sensing technologies. The spectral reflectance obtained by UAV and the chlorophyll fluorescence measured by a handheld sensor were used to analyze the spatial dynamics and the photosynthetic functions of the kudzu community.

I conducted three experiments at the riverbank of Ina City, Nagano Prefecture, Japan. First, the seasonal change of growth and spatial distribution were evaluated by UAV image processing. The occupancy in each grid was classified based on the brightness of the red, green and blue (RGB) image and the colonization rate in each period was calculated. To evaluate the growth and spatial distribution, the LAI was estimated from

spectral reflectance. Secondly, the spatio-temporal model of the community dynamics was constructed based on the time-series spatial occupancy data. The influence of disturbance on kudzu community dynamics was evaluated through the values of the evaluated parameters obtained in each period. Thirdly, the effect of leaf orientation on light interception and the photosynthetic function of kudzu was evaluated through measurement of chlorophyll fluorescence using a portable fluorometer.

Structure

Chapter 2 describes my evaluation of the spatial distribution of the kudzu community using aerial image processing. I estimated the presence or absence and the LAI of kudzu from the spectral reflectance obtained by UAV to evaluate the growth and expansion of the kudzu community.

Chapter 3 describes my evaluation of kudzu community dynamics using aerial image processing and the hierarchical Bayesian model. The occupancy states of each grid on the UAV image were applied to a hierarchical stochastic model and the parameters on emergence and expansion were inferred by the Markov chain Monte Carlo method.

Chapter 4 describes my investigation of the influence of leaf orientation on radiation interception and photosynthesis of the kudzu canopy. The light acclimation mechanisms of the kudzu canopy were revealed by assessing the leaves using a portable spectrophotometer, which can quickly measure environmental and photosynthetic parameters.

Chapter 5 consists of a general discussion on three topics. First, the ecological traits and optimal management of kudzu are discussed based on the results of the three studies. It also discusses the benefits and application of remote sensing and modeling for weed ecology. Finally, I present the feasibility of further extension of sensing and modeling in weed ecology.

Chapter 2

Classification and analysis of the spatial distribution of kudzu community using aerial image processing

Abstract

The aim of this study was to evaluate the spatial distribution of the kudzu community based on grid-based unmanned aerial vehicle (UAV) imagery processing. High-resolution RGB and multispectral images of the riverbank (40 m × 30 m) were obtained from a 50-m altitude five times from June to October 2018. Orthomosaic images were generated and divided into 3221 grids (50 cm × 50 cm). The support vector machine classifiers trained by 5% of the grids successfully classified all the grids into two classes (presence/absence) (accuracy > 0.9, F-measure > 0.9) except for June 4. In addition, multiple regression models to estimate leaf area index (LAI) from three vegetation indices were employed for each observation (adjusted R^2 = 0.421–0.570) except for October 2. The LAI decreased in the center of the kudzu community from July to August, and clusters of high LAIs moved from the center to the outer margins of the community. At the same time, the spatial distribution of the LAI became uniform. This change may be attributed to the spread of leaves on higher-order branches during the renewal of leaves in summer. The community expanded quickly after mowing at the end of July, indicating that the shoots that newly emerged from the residual overwintering stems and the crowns grew quickly and compensated for the damage. These results indicate that time-series UAV imagery is useful in evaluating the spatial growth and distribution of weed communities.

Abbreviations

SVM - support vector machine

LAI - leaf area index

TP - true positive

FP - false positive

FN - false negative

TN - true negative

NDVI - normalized difference vegetation index

NDRE - normalized difference red edge

SAVI - soil adjusted vegetation index

Introduction

Extraction of target species information from vegetation is a complicated process. Manual classification involves the construction of certain criteria through cognitive processes in their brain. Supervised learning can construct classification criteria flexibly and seems to be suitable for grid-based UAV image classification. Parameters are not necessarily assumed to have normality. Non-parametric methods do not require assumptions on normality and therefore, are suitable for building classifiers based on many different types of data. Many kinds of non-parametric methods, such as the k-nearest neighbor algorithm (k-NN) and artificial neural network (ANN), have been proposed for use. Especially, support vector machine (SVM) is suitable for standardization and labor-saving of classification. It generates a maximum-margin hyperplane in feature space by kernel trick based on a set of labeled training data and constructs a robust classifier flexibly to the data (Araki 2014). Classification of weed requires the segmentation of each grid based on slight differences in the color of leaves between species, which will change by season. In addition, the brightness of each band in each grid is affected by weather conditions and time. Such classification will be achieved by maximizing the margin between a hyperplane and each cluster by SVM built in each observation. Consequently, SVM has been recruited for weed detection and has relatively higher accuracy than the other methods of supervised learning (Alexandridis *et al*. 2017, Zheng *et al*. 2017, Bakhshipour and Jafari 2018).

Spectral reflectance has been utilized as a parameter in remote sensing of vegetation. Chlorophylls absorb red and blue rays while it reflects green rays partially and near-infrared (NIR) rays strongly. Based on this phenomenon, many kinds of vegetation indices have been proposed. For example, normalized difference vegetation index (NDVI) (Rouse *et al*. 1974) is calculated from the reflectance of red and near-infrared ray. Reflectance in red edge, a narrow band between red and NIR, has been proved to reflect the chlorophyll content (e.g., Horler *et al.* 1983) and also has been utilized.

The process in which the plant expands to the other grids can be described in the model stochastically. The model based on the location of individual plants and the distance between them has been generally used to evaluate the expansion rate of a community (Shigesada 1992). The expansion rate of the kudzu community can be based on the area of the grids classified to be occupied. However, the expansion rate of the community's margin is important for exclusion from virgin territories such as farms or

roads. Komuro and Koike (2005) evaluated the expansion of shrub species in the suburban area using a colonization kernel that represents the relationship between colonization probability and distance. By adopting a similar kind of kernel to grid-based presence/absence data, the expansion rate of a community's margin can be evaluated quantitatively and compared among different periods or managements. For the evaluation of spatial distribution, it is appropriate to estimate the LAIs of the grids in which the presence of kudzu is identified. Spatial distribution has been investigated from surface data of vegetation both statically and dynamically. Many models and indicators have been proposed for static analysis in plant ecology and grassland science. Spatial autocorrelation is evaluated based on distance and indicates spatial agglomeration of value. In particular, local indicators of spatial association (LISA) is used for spatial agglomeration (Anselin 1995).

This chapter evaluates the spatial dynamics of a kudzu-dominated community based on time-series UAV imagery. Aerial images of the plant community including kudzu a the riverbank were obtained sequentially by UAV. The images were divided into grids, and whether kudzu was present/absent was identified using supervised learning. The area occupied by kudzu was calculated and the expansion rate of the community's margin was evaluated using colonization kernel. At the same time, the linear model for estimation of the leaf area index (LAI) of the community from the spectral reflectance was constructed. Based on the estimated LAI, the growth rate was measured and the spatial heterogeneity and spatial autocorrelation were evaluated.

Materials and Methods

Location and management of the study site

The study was conducted at the bank of Mibu River in Ina City, Nagano Prefecture (Fig 2-1). The experimental field (35.823 °N, 137.992 °E, 60 × 40 m) was dominated by kudzu and also grew eulalia grass (*Miscanthus sinensis* Andersson) and Japanese mugwort (*Artemisia princeps* Pampan). The experimental area was surrounded by the shrubs of black locust (*Robinia pseudoacacia* L.) and indigo bush (*Amorpha fruticosa* L.). These shrubs were excluded before the identification of kudzu because they could easily be identified visually or by the digital surface model (DSM).

The surveys were conducted on June 4, July 2, July 20, August 18, and October 2,

2018, indicative of the period of the beginning of the annual growth of the stem, stem elongation, the peak of leaf expansion, the slowdown of stem growth, and the transport of carbohydrate to the root, respectively (Obayashi 1979, Tsugawa and Kayama 1981a, Rashid *et al.* 2017). The field was passed through by a passage and the kudzu in the margins of the passage were trampled and removed using a backhoe at the end of July.

Data collection

Aerial 8-bit RGB and multispectral images were obtained by the RGB camera Zenmuse X4S (DJI) and multispectral camera Parrot Sequoia (Parrot) mounted on UAV Inspire 2 (DJI) in the daytime (around 10 am) on sunny days from June to October 2018. The UAV flew at an altitude of 50 m automatically to obtain RGB images with 80% front and side overlap by GS Pro (DJI), while the multispectral camera measured the reflectance of 4 bands (Green: 550 ± 40 nm, Red: 660 ± 40 nm, Red edge: 735 ± 10 nm, Near-infrared: 790 ± 40 nm) at intervals of 3 s, simultaneously. The resolution of the RGB and the multispectral images were 1.65 and 4.68 cm/pixel, respectively. Kudzu's leaflet is known to become parallel to solar radiation in the daytime (Liu *et al.* 1997a) and was difficult to recognize in the images obtained at around 10 am. Therefore, the RGB images obtained in the twilight were adopted for the detection of kudzu. However, the spectral reflectance at around 10 am was adopted for estimation of the LAI.

The aerial images were integrated into orthomosaic images and calibrated by the image processing software Pix4Dmapper (Pix4D). The location was calibrated based on the conspicuous structures (fences or blocks) in the images, and the coordinates of the point (rectangular plane VIII) were acquired from the website of Geographical Survey Institute (Geographical Survey Institute 2019). The brightness was calibrated based on calibrated reflectance panels in the images.

Furthermore, the LAI was measured by sampling in 10 quadrats of 50 × 50 cm area. The LAI on July 20 was measured in 9 quadrats because the measurement was not precise in one quadrat.

Detection of kudzu

The presence or absence of kudzu in all the girds was identified visually based on whether or not 50% of the grid of 50 × 50 cm was occupied by kudzu leaves. In the

general vegetation survey (Nemoto 2001), the coverage is evaluated in units of a quadrat with 1–2 m on each side. This study aimed to classify the presence/absence in each grid and evaluate the spatial distribution of kudzu, hence, did not consider the coverage inside each quadrat. Furthermore, the reflectance of each kudzu leaf may not influence the reflectance of the grid, and the grid may be classified as absent in case the grid is too large compared to the leaflet of kudzu (approximately 15 cm diameter). Therefore, each grid was made 50 × 50 cm and was classified as "present" when kudzu covered over half of the grid.

The orthomosaic images were split into 3221 grids of 50 × 50 cm in the GIS software ArcMap (ESRI). The grids were classified into two classes (presence/absence) by SVM, based on the brightness of each band of the RGB images. 1, 2, 5, 10, 20, 50% of all the grids were extracted randomly to train classifiers for each observation. Supervised learning underwent 10 times per observation by the ksvm function in the kernlab package (Karatzoglou *et al*. 2004) of **R** ver. 3.4.4 (R Core Team 2019) (Kin 2017). In this classification by SVM, a linear classifier was applied instead of the conversion of variables.

For evaluation of the classification, Accuracy and F-measure were calculated (Araki 2014). Accuracy is the ratio of the data classified correctly to all the data and defined as follows:

$$Accuracy = \frac{TP + TN}{TP + FP + FN + TN}$$

where TP is the number of true positives, FP is the number of false positives, FN is the number of false negatives, and TN is the number of true negatives.

F-measure was calculated as an indicator of the balance of Precision and Recall. Precision and Recall are defined as follows:

$$Precision = \frac{TP}{TP + FP}$$

$$Recall = \frac{TP}{TP + FN}$$

To quantify the expansion of the community, it is important to acquire the area occupied in each observation as precisely as possible. There exists a trade-off between $Precision$ and $Recall$. The expansion rate cannot be measured precisely when the classifications are too active or too passive. Therefore, I calculated $F-measure$ as an indicator to certify that the classifier is not too active or too passive to classify kudzu's presence. $F-measure$ is a harmonic mean of $Precision$ and $Recall$ and is defined as follows:

$$F-measure = 2 \times \frac{Precision \times Recall}{Precision + Recall}$$

Spatial occupancy and expansion

Based on the result of the classification supervised by the data of 161 grids (5% of all the grids), the expansion rate of the community's margin in 3 plots under different management in two periods (July 2–July 20 and August 18–October 2) were evaluated and compared. The period of July 20–August 18 was excluded from the evaluation because the community became too small to trample using a backhoe. All the 3 plots were located on the margin of the community. Plot A was located in the north of the community and faced the promenade. At the end of July, Plot B and C were trampled using a backhoe along the width of 1 m and 3 m from the edge of the community, respectively.

A negative-exponential function of distance was used to approximate the colonization kernel (Komuro and Koike 2005). The distance of the nearest source grid (the grid occupied by kudzu at the previous observation) to every grid in the plot, r, was measured (Fig. 2-2). The probability that kudzu exists at the end of the period, $\mathrm{z}(r)$, is regarded to follow a negative-exponential function and is defined as follows:

$$z(r) = \frac{1}{1 + e^{kr+l}}$$

where k and l are regression coefficients. The parameters were estimated using the `glm` function of **R**. The object variable was the binary data of kudzu's presence/absence in each grid at the end of the period, and the explanatory variable was r. The probability distribution was binomial distribution.

For interpretation of the parameters, the probability that kudzu exists in the source grid $(r = 0)$ at the end of each period, Z_0, is defined as follows:

$$Z_0 = \frac{1}{1 + e^l}$$

The distance at which $z(r)$ decreases to half of Z_0, $D_{0.5}$, is defined as follows:

$$D_{0.5} = \frac{ln(2 - Z_0) - ln(1 - Z_0)}{k}$$

$D_{0.5}$ was utilized as an indicator of colonization by each woody species by Komuro and Koike (2005). We used $D_{0.5}/day$, a quotient of $D_{0.5}$ divided by the number of days of the period, as an indicator of the edges' expansion rate because the intervals of observation were not even in this study.

Estimation of LAI

The normalized difference vegetation index (NDVI), normalized difference red edge (NDRE), and soil adjusted vegetation index (SAVI) were calculated from multiple spectral reflectance.

The NDVI was calculated from the reflectance of red and near-infrared rays. It has been utilized to estimate the LAI and biomass (Rouse *et al*. 1974). It is defined as follows:

$$NDVI = \frac{NIR - R}{NIR + R}$$

where NIR is the near-infrared reflectance and R is the red reflectance.

The NDRE reacts sensitively to chlorophyll (Gitelson and Merzlyak 1997) and is defined as follows:

$$NDRE = \frac{NIR - RE}{NIR + RE}$$

where RE is the red-edge reflectance, which is sharply affected by chlorophyll concentration in the leaf.

The SAVI was proposed to reduce the influence of soil' reflectance (Huete 1988) and

is defined as follows:

$$SAVI = \frac{(1+L)(NIR-R)}{NIR+R+L}$$

where L is an adjustment factor based on LAI values; $L = 0.5$ was adopted in this research because the adjustment factor of $L = 0.5$ was found to reduce soil noise problems substantially for a wide range of LAI values (Huete 1988). The orthomosaic images of these three VIs were fed into ArcMap (ESRI) and the mean of each quadrat's VI was calculated. The multi regression models were constructed by the `lm` function of **R** to estimate LAI. The objective variable was the LAI of each quadrat, and the explanatory variables were the three VIs. The models were selected stepwise based on AIC, using `stepAIC` functions in the `MASS` package (Venables and Ripley 2002) of **R**. The goodness of fit of the model was evaluated by adjusted coefficient of determination (adjusted R^2).

The LAIs in the grid in which kudzu were speculated to be present by SVM were estimated by the model. The LAIs on June 4 were estimated in the grid in which kudzu was estimated to be present manually because the occupancy could not be judged accurately by supervised classification. The LAIs on October 2 were not estimated because the goodness of fit of the model was not enough. In addition, the LAI growth rates (= differentiation of LAI / days) of each grid were calculated in the three periods (June 4–July 2, July 2–July 20, and July 20–August 18). The LAIs of the grids in which kudzu was estimated to be absent were regarded as zero. The growth rate in the period from August 18 to October 2 could not be calculated because the LAI could not be estimated accurately on October 2.

It should be noted that spectral reflectance includes the reflectance of plants other than kudzu too. It is technically difficult to acquire the spectral reflectance of kudzu alone from a complicated community with multiple weed species. The estimated values of LAI should be regarded as the LAI of the kudzu-dominated community.

Spatial distribution of LAI

Hot spots (the places where high values of LAI cluster intensely) and cold spots (the places where low values of LAI cluster intensely) were specified by the `localG` function

of spdep package (Bivand and Wong 2018) of R. Getis-Ord G_i^* is one of the indicators of local spatial autocorrelations (Getis and Ord 1992) and is calculated as follows:

$$G_i^* = \frac{\sum_j w_{ij} y_j}{\sum_j y_j}$$

where y_j is the estimated LAI of the grid j and w_{ij} is the parameter representing the dependence of grid j on i. In this study, to take account of only the nearby grids, we considered $w_{ij} = 1$ when the distance between grid j and i was less than 3 and $w_{ij} = 0$ when the distance was more than 3. The grids with a significantly high or low value of G_i^* were regarded as hot spots and cold spots, respectively.

Results

Detection of kudzu

Fig. 2-3 shows the $Accuracy$ and $F-measure$ of the classification by SVM. The result of June 4 was omitted from Fig. 2-3 because no grid was classified into presence and $F-measure$ could not be calculated. The $Accuracy$ of classification was mostly higher than 0.9 in the other observations, but those on July 2 and October 2 were lower than 0.9 in a few trials when 1%–2% of all the grids were used for classifier training. $F-measure$ of classification was mostly higher than 0.9 except on June 4, but that on October 2 was lower than 0.9 for the relatively low $Accuracy$ in a few trials. The $F-measure$ of classification on October 2 was sometimes lower than 0.9 because the $Precision$ was relatively lower.

The grids dominated by bur cucumbers (*Sicyos angulatus* L.), Japanese hops (*Humulus scandens* (Lour.) Merrill), giant ragweeds (*Ambrosia trifida* L.), and eulalia grasses were sometimes misclassified to be occupied by kudzu. In addition, the grids in which *Artemisia* spp. existed and the coverage was high were sometimes misclassified to be occupied by kudzu.

To ensure enough $Accuracy$ and $F-measure$ of classification, the results by a classifier trained by the brightness of the 161 grids (5% of all the grids) were submitted for the evaluation of the community's spatial occupancy four times from July 2 to October 2. The results of the manual classification were submitted on June 4.

Spatial occupancy and expansion

Fig. 2-4 shows the grids classified to be occupied by kudzu in each observation. There were several small patches (smaller than 10 m^2) on June 4 and grew to fill in the gap and formed a large community (approximately 400 m^2 on the north and 80 m^2 on the south of the passage) by July 2. The kudzu on both sides of the passage were removed by the end of July.

After mowing at the end of July, the community expanded but the loss of area was not compensated by October. Table 2-1 represents the expansion rate and the relative expansion rate of the area occupied by kudzu based on the results of the classification. The expansion rate and the relative expansion rate in the period from June 4 to July 2 were 8.94 m^2/day and 0.0338 /day, respectively. They were the highest values in the season. The decrease in the community's area in the period from July 20 to August 18 was due to the removal of kudzu.

Fig. 2-5 shows the regression curve representing the relationship between the probability of kudzu's presence $\mathrm{z}(r)$ and the distance from the nearest source grid *r*. The community expanded and $D_{0.5}/day$ was 0.0212–0.0470 m/day in the period of leaf expansion (July 2–July 20). In the period of carbohydrate accumulation (August 18–October 2), $D_{0.5}/day$ was higher (0.0574 m/day) than in the period of leaf expansion in plot C, while it was lower in Plot A and B.

Estimation of LAI

Table 2-2 shows the multiple regression models to estimate LAI from VIs and their adjusted R^2. The adjusted R^2 was 0.551 and 0.570 on July 20 and August 18, respectively, and 0.421 and 0.444 on June 4 and July 2, respectively. On October 2, it was difficult to estimate LAI as the adjusted R^2 was 0.140. SAVI was adopted four times from June to August, while NDVI was adopted only on June 4 and NDRE on June 4 and July 2.

Spatial distribution of LAI

Fig 2-6 shows the estimated LAI of each grid based on the models on June 4, July 2, July 20, and August 18. The LAI increased from June to July but decreased in the center of the community and increased at the margin by August.

Fig 2-7 shows the distribution of the growth rate of the estimated LAI. The growth rate was positive in the wide range from June 4 to July 2. It was negative at the margin of

the community from July 2 to July 20, while it was higher than 0.30 d^{-1} in the center. Some grids had a positive growth rate at the margin from July 20 to August 18 and negative in the center.

Fig 2-8 shows the distribution of Getis-Ord G_i^* of the estimated LAI in each period. The hot spots were located in the center of the community from June 4 to July 20 but gradually translocated and localized at the community's margin on August 18.

Discussion

The classifiers trained by the brightness values of 5% of the grids in each observation achieved an accuracy of over 0.9 and an F-measure of over 0.9, except on June 4 (Fig. 2-3). This shows that the community of target weed can be detected using aerial imagery by employing small training data. This result indicates that supervised classification by SVM is useful in classifying the presence/absence of kudzu after July.

It was difficult to classify kudzu accurately in June because the shoots emerging from the nodes of the overwintering stems had not grown, and other species that had already started growing, such as *Artemisia* sp., were dominant. Therefore, for classifying weed at the early stage of growth, it should be acceptable to adjust grid size to make it smaller or introduce object-based classification. Multispectral reflectance might be valuable to raise the accuracy of classification. The stems of kudzu climb other plants and leaves spread on the surface of canopies after July, indicating that the reflectance of kudzu leaves affects the brightness of each grid more than before. Bur cucumber and Japanese hop have climbing stems, and giant ragweed and eulalia grass are tall; these species can spread leaves on the surface of canopies after July, and therefore, it is important to distinguish kudzu from them.

My method seemed to be suitable to detect kudzu after coverage of canopies but there was still room to improve ways to distinguish kudzu from the other plants. Features other than the brightness of RGB imagery should be utilized to distinguish species more accurately. Suzuki *et al.* (2010) constructed a linear model based on the hyper spectral images obtained on the ground and distinguished grasses, legumes, and other weeds. In particular, the reflectance of the red edge (680–750 nm) seems to be effective for its reaction to chlorophyll content (Gitelson *et al*. 1996). In addition, the shape and texture of plants may be useful features for identification. Oguma *et al.* (2016) used not only the brightness but also the connectivity of pixels of leaves and flowers as a feature and

successfully reduced the misclassification of flowers. Furthermore, conversion of nonlinear data to linear by kernel function may also be useful (Kin 2017).

For LAI estimation, SAVI was incorporated into the models in all observations, whereas NDVI was adopted only on June 4. SAVI increases linearly with increasing LAI and NDVI saturates at high LAI by reflectance on the ground in crops (cotton, maize, wheat, soybean) (Huete 1988, Haboudane *et al*. 2004). NDRE does not seem to reflect leaf area after July possibly because the chlorophyll content of each leaf is not uniform in a quadrat. Vertical variation in the chlorophyll content in the canopy might become heterogenous in the process of leaf regeneration after July; regardless, all the leaves were taken into account to measure the area.

On October 2, dead leaves that were not included in the leaf area in the quadrats seemed to prevent estimation of LAI. The adjusted R^2 was not as high in this study compared to previous studies. For example, the coefficient of decision in the LAI estimation of the community at the riverbank dominated by kudzu and reed (*Phragmites japonica* Steud.) was reported to be 0.70 by Takahashi and Yasuoka (2006). The precision of estimation will depend on the other species in the grid and canopy architecture in the surrounding grids. For improving estimation, it might be effective to adjust the size of the grid to canopy architecture and species composition and to incorporate error factors into the model. Additionally, it might be better to build a flexible model by generalized linear model or machine learning for the evaluation of spatial distribution from the estimated LAI.

The occupied area increased rapidly, filling the gaps among small patches with newly expanded leaves by July, and the LAI increased. Thereafter, the community did not expand, except in the mowed area, while the LAI decreased in the center and increased at the margin. The leaves were dead especially at the lower level of the canopy in the field in August. These facts indicate that the LAI was translocated from the center to the margin after July. Leaves seem to renew from July to August, when the LAI growth rate per annual shoot is relatively small (Tsugawa and Kayama 1981a). Kudzu extends mainly main stems and low order branches from June to July and high order branches from August to September (Tsugawa and Kayama 1981a, b). Therefore, kudzu seems to remove leaves mainly from the main stems and lower order branches in the center of the community after July and expand new leaves on higher-order branches at the margin by October. Generally, the spatial distribution of herbaceous plants depends on propagation

type. The distribution of clonal plants is aggregated, while non-clonal plants distribute uniformly (Tsutsumi *et al*. 2001, Yasuda *et al*. 2003). The process of propagation without dispersal, such as branching and elongation of the stem, generates aggregated distribution (Iwasa *et al.* 1977). The spatial distribution of leaves in July was aggregated seemingly because kudzu spreads its leaves in the neighborhood in the process of stem expansion. However, the defoliation in the center and expansion of new leaves at the margin seem to make the spatial distribution uniform in the summer.

The margin of the community spread during the period of leaf expansion (July 2–July 20). In the period of carbohydrate accumulation, the expansion rate was lower than that in July in Plot A and B, while the area of the community recovered quickly in Plot C after mowing. This suggests that kudzu spreads its community rapidly by lower-order branches until the period of the leaf expansion and slowly as the higher-order branches grow during the transportation of photosynthetic products into storage organs. In Plot C, many overwintering stems and crown roots were left after mowing. These might have small shoots that are hardly detected in UAV imagery. In addition, artificial defoliation in the summer increases higher-order branches (Frye and Hough-Goldstein 2013). Therefore, the removal of leaves and stems might have promoted the development of higher-order branches. The expansion rate of the community is slower in July than in September' kudzu compensates for this damage by the emergence of new shoots from residual overwintering stems and crown roots and extension of high order branches from residual stems in case the margin of the community is mowed.

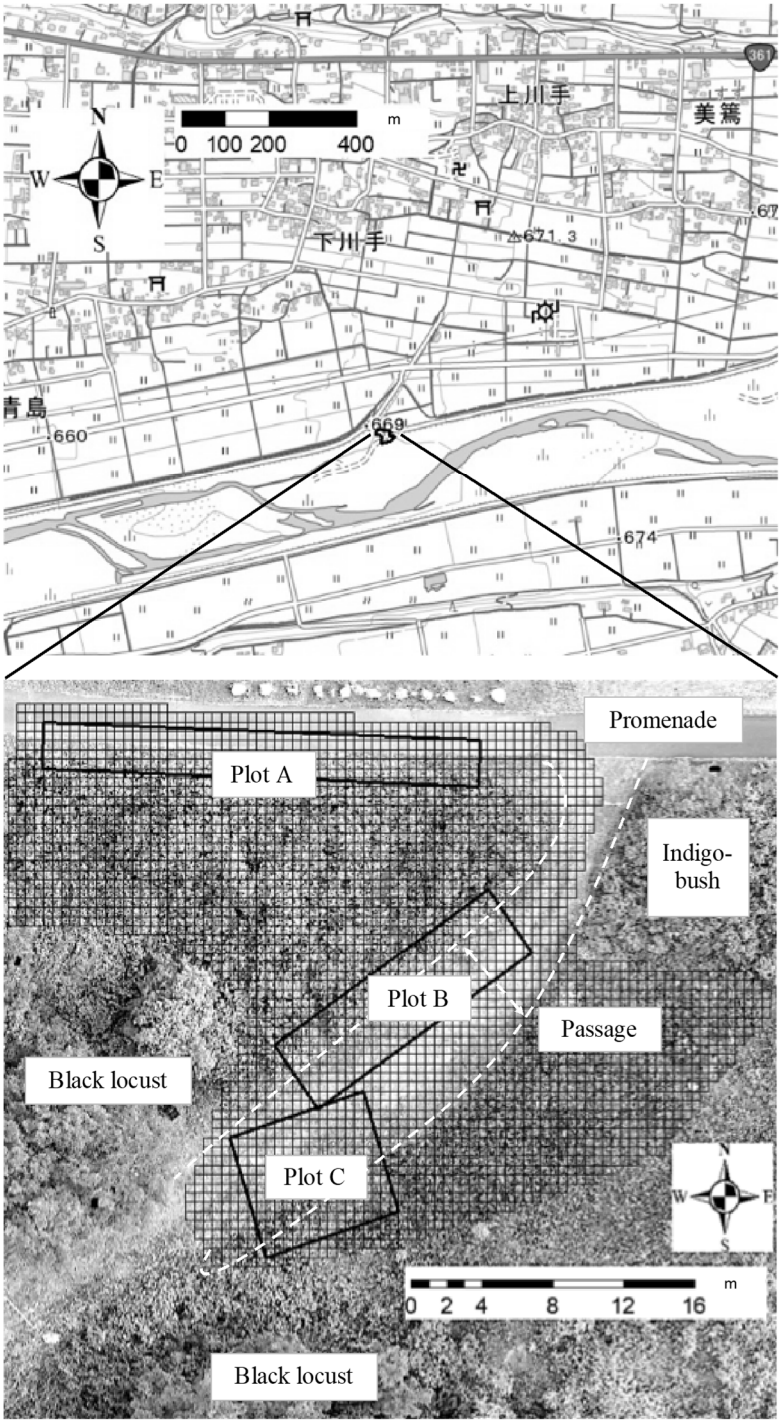

Fig. 2-1

Location of the experimental areas at the riverbank of Mibu River.

The map (above) is based on a digital map published by the Geospatial Information Authority of Japan.

The aerial image (below) was obtained soon after mowing on August 18, 2018.

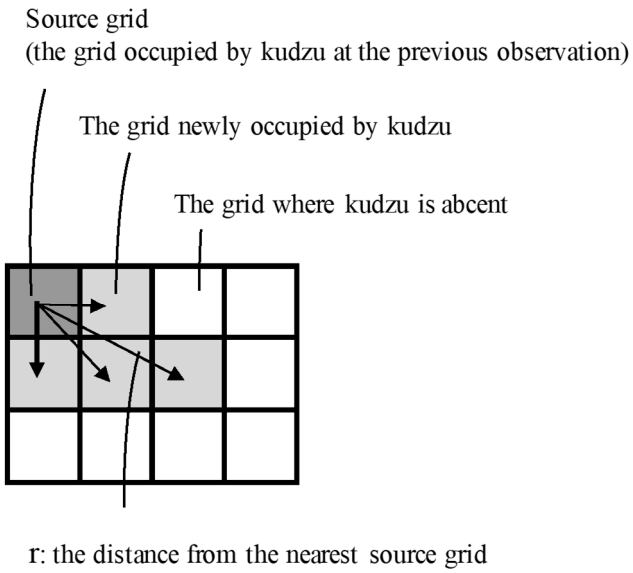

Fig. 2-2

The definition of the source grid and the distance of the colonization kernel.

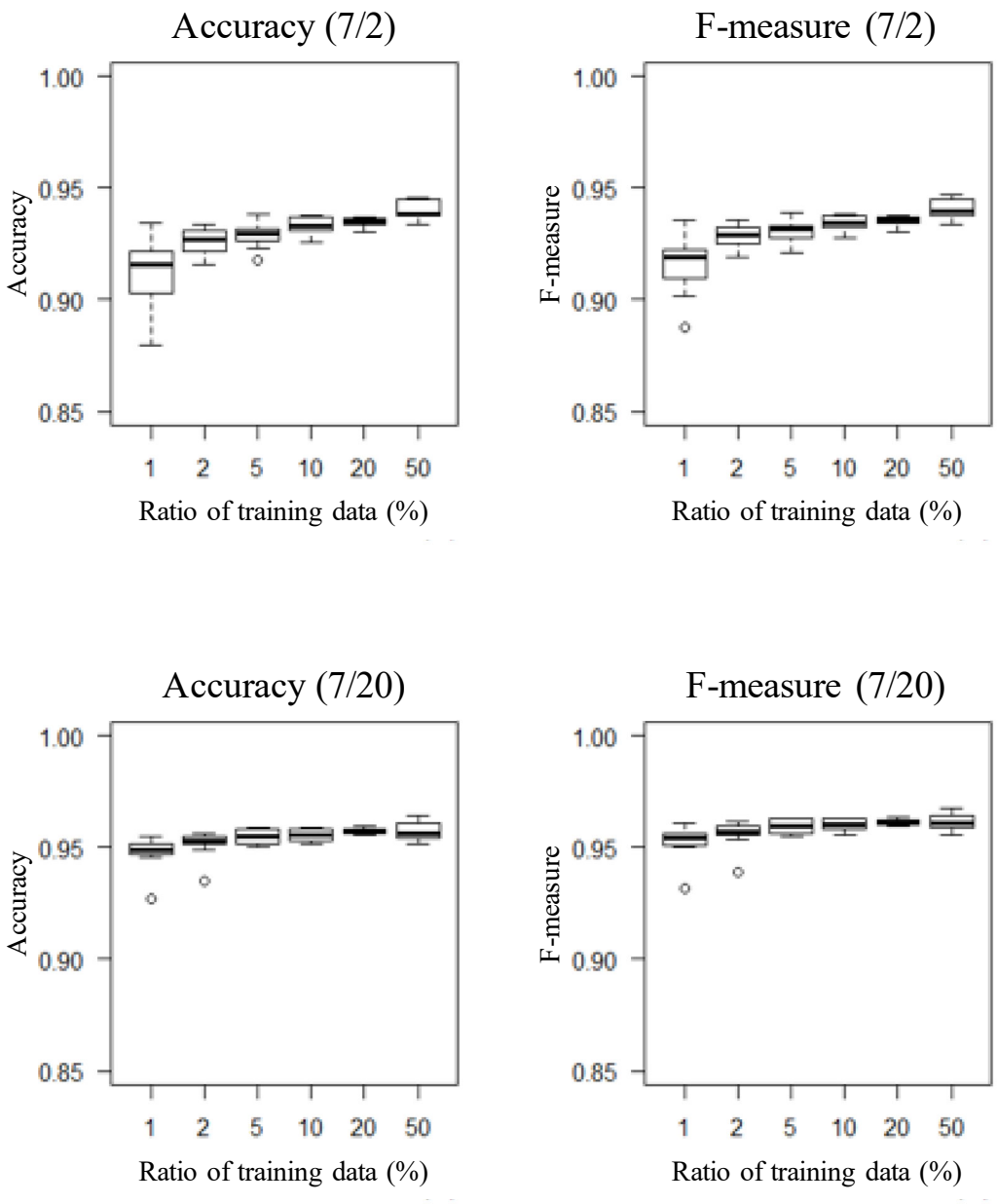

Fig. 2-3

The Accuracy and F-measure of classification by support vector machine.

The line in the box indicates the median, the box indicates the first and third quantiles, and the whiskers indicate the highest/lowest value that is within 1.5 times the interquartile range from the box. The outliers indicate the data beyond the end of the whiskers.

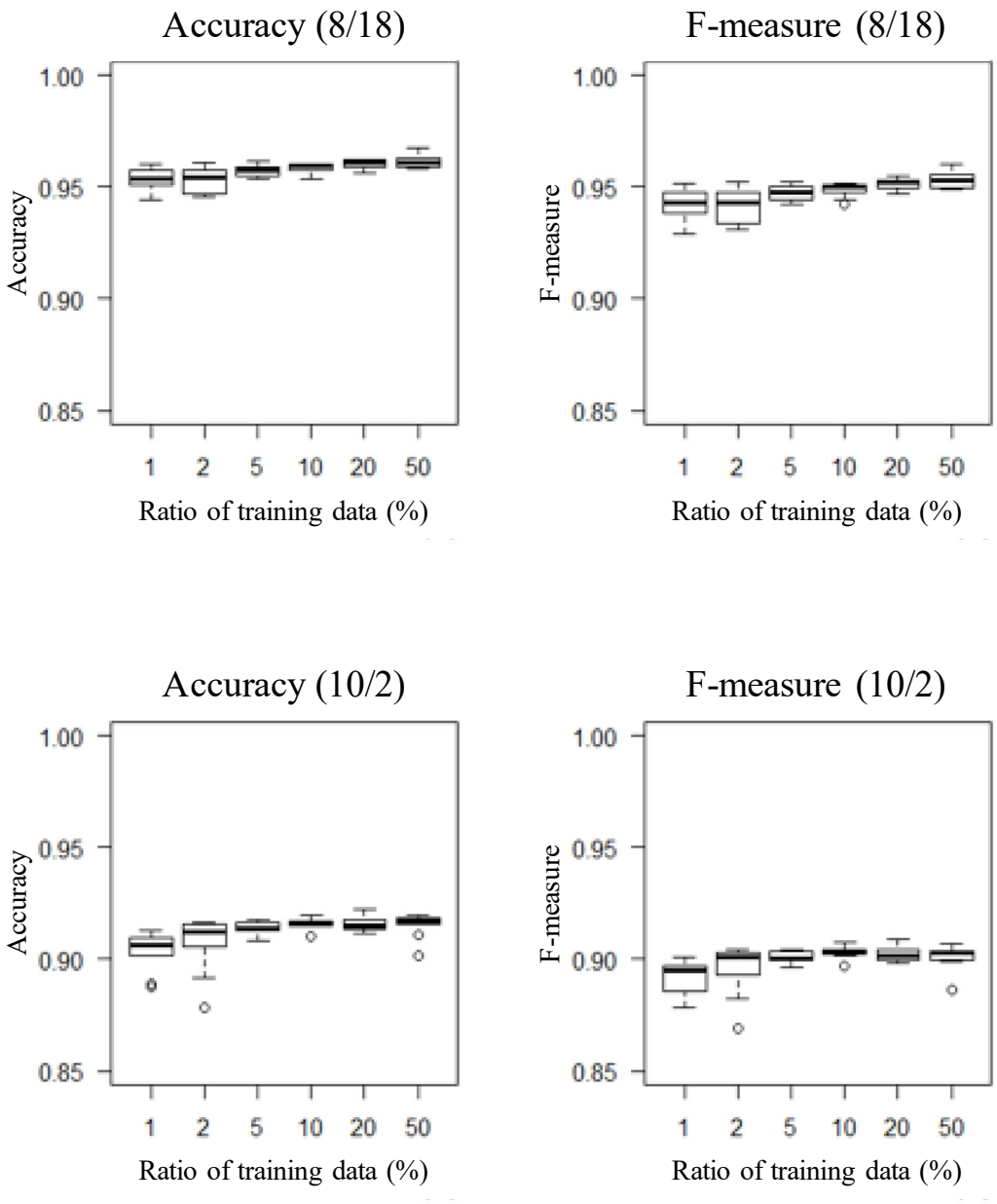

Fig. 2-3 (continued)

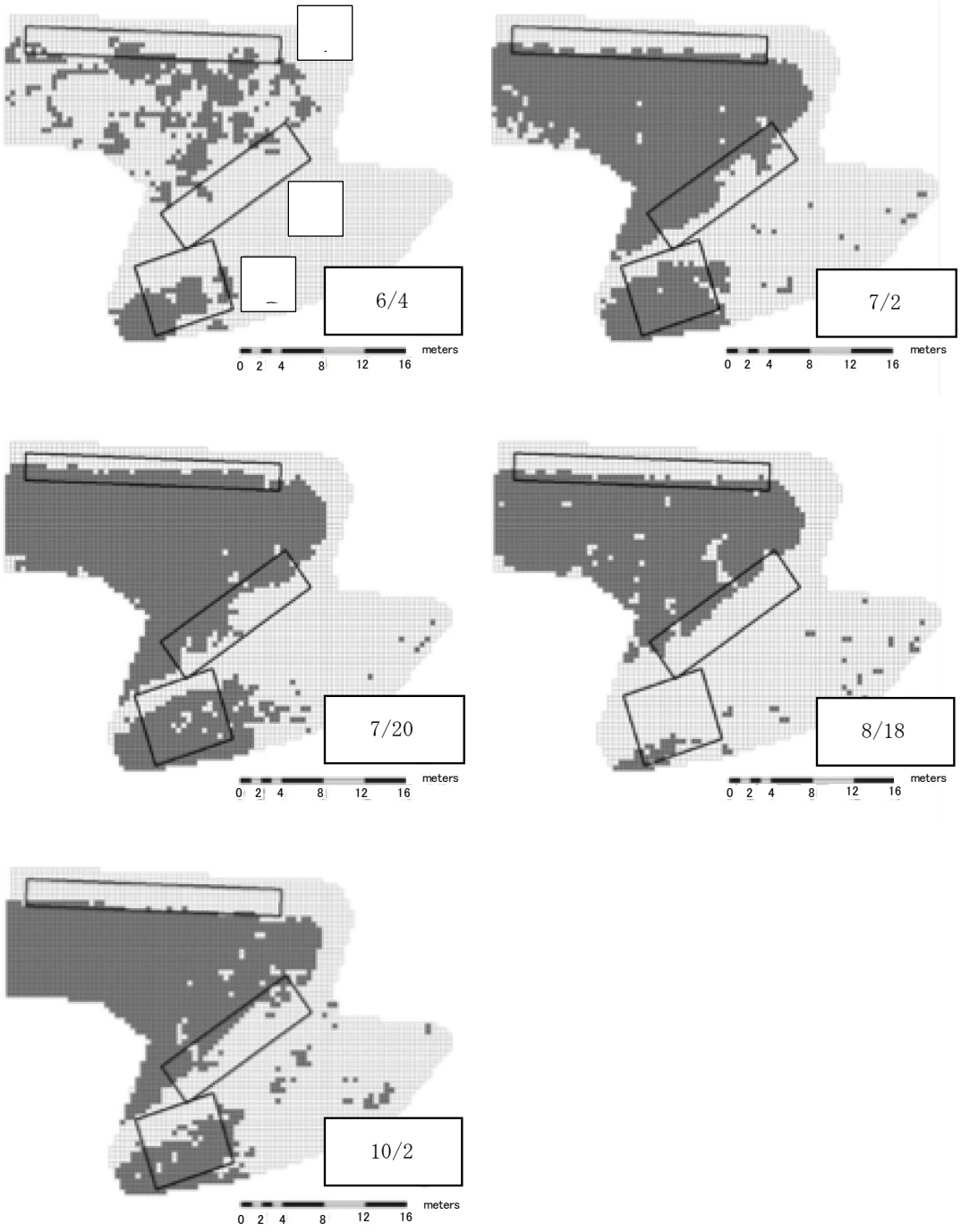

Fig. 2-4

The area occupied by kudzu classified 5% of all the grids.

The shaded grids were manually classified to be occupied by kudzu on June 4. The others were classified by support vector machine.

Table 2-1

The expansion rate and relative expansion rate of the area occupied by kudzu.

The expansion rate and relative expansion rate between July 20th-August 18th were negative because the kudzu at the margins of the passage were trampled and removed by a backhoe.

	Area (m^2)	Expansion rate (m^2 / day)	Relative expansion rate (/ day)
6/4	159		
		8.94	0.0338
7/2	409		
		2.40	0.0056
7/20	452		
		-4.36	-0.0113
8/18	326		
		1.32	0.0037
10/2	385		

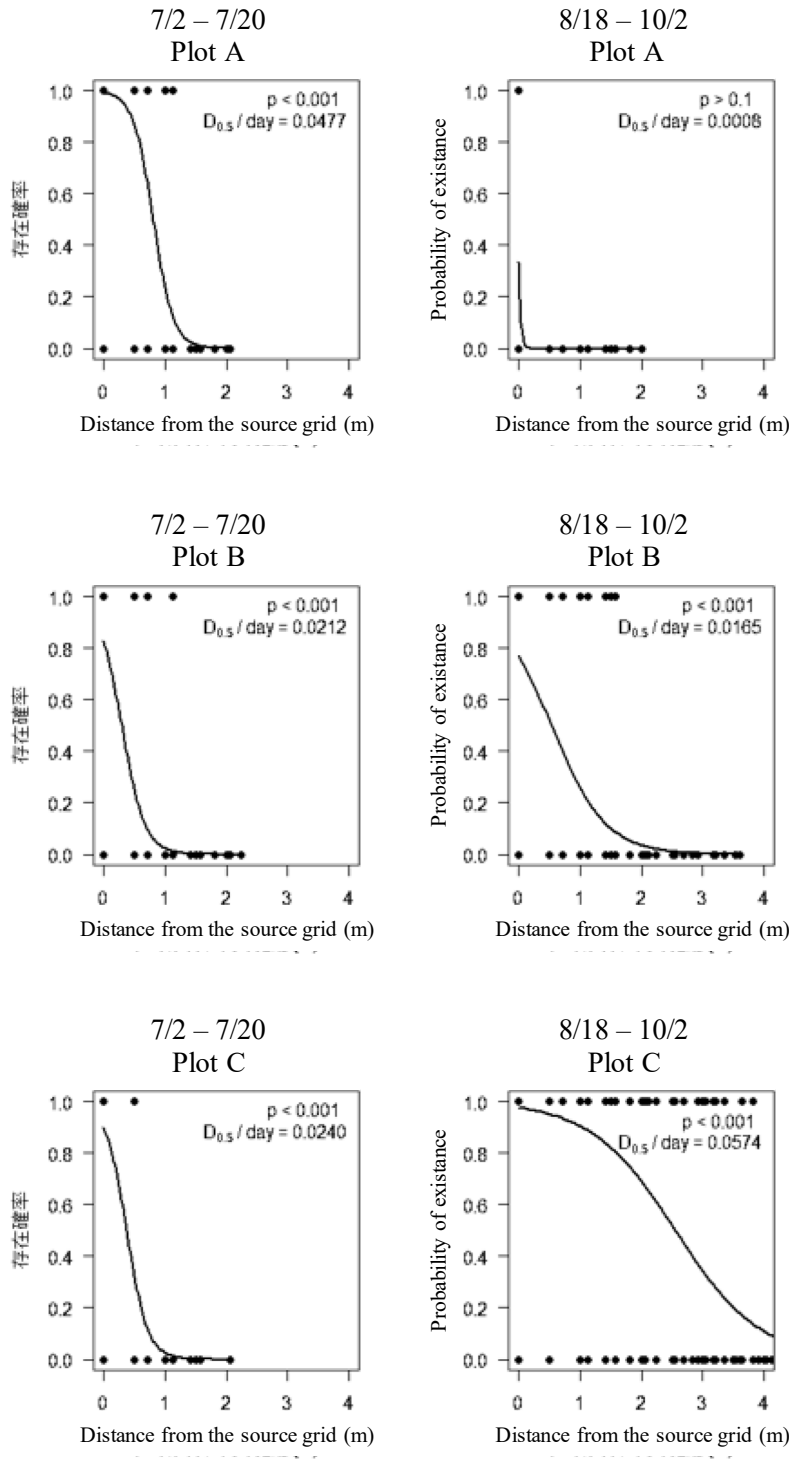

Fig. 2-5

The colonization kernels, p-value, and $D_{0.5}$/day (m/day).

Leaf expansion: July 2–July 20; Carbohydrate storage: August 18–October 2.

Table 2-2

Regression coefficients, p-value, and adjusted R^2 of a leaf area index (LAI) estimation model for each observation.

Date	Explanatory variable	Regression coefficients	p-value	Adjusted-R^2
6/4	(Intercept)	2.31	0.44	0.44
	NDVI	-9.76	0.13	
	NDRE	17.11	0.18	
	SAVI	10.62	0.09	
7/2	(Intercept)	-8.60	0.09	0.42
	NDVI	-	-	
	NDRE	12.43	0.17	
	SAVI	11.28	0.07	
7/20	(Intercept)	-42.54	0.02	0.57
	NDVI	-	-	
	NDRE	-	-	
	SAVI	76.34	0.01	
8/18	(Intercept)	-7.11	0.04	0.55
	NDVI	-	-	
	NDRE	-	-	
	SAVI	21.00	0.01	
10/2	(Intercept)	-0.08	0.99	0.14
	NDVI	0.00	0.26	
	NDRE	-0.47	0.08	
	SAVI	0.00	0.26	

NDVI, NDRE and SAVI mean normalized difference vegetation index, normalized difference red edge and soil adjusted vegetation index, respectively.

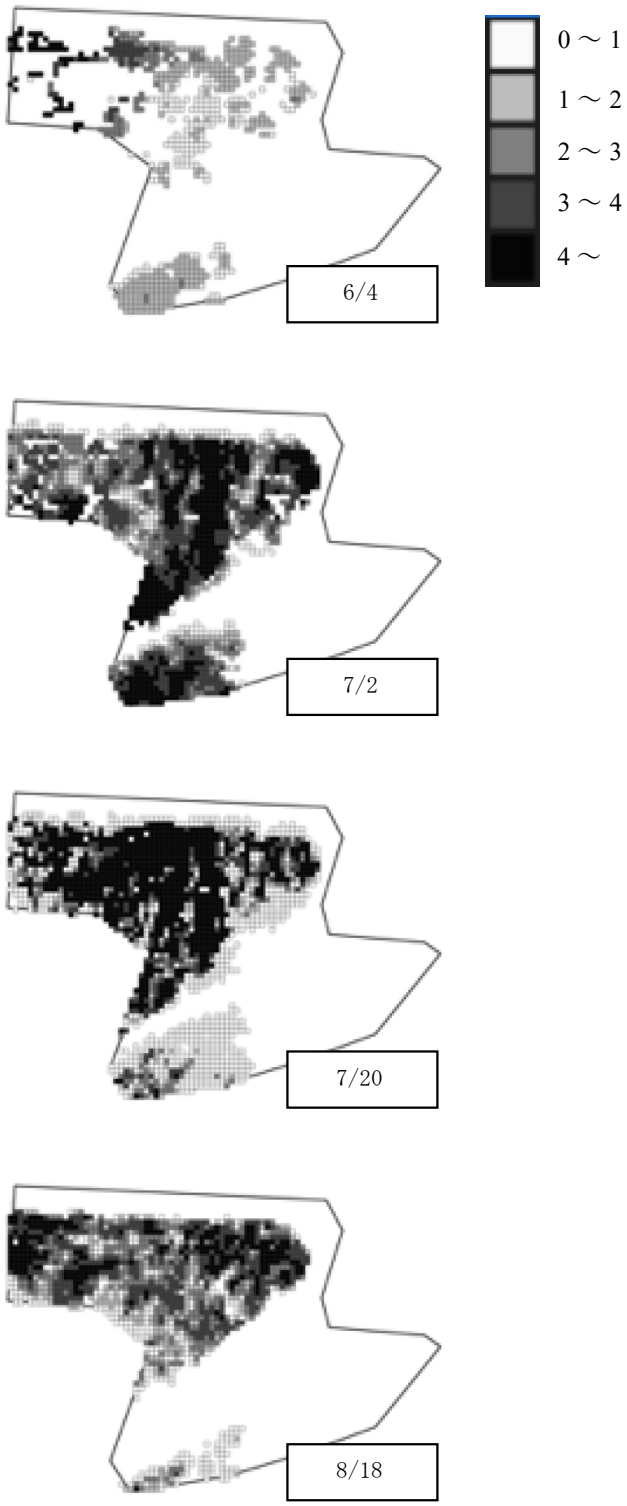

Fig. 2-6

Transition of estimated leaf area index (LAI) in each 50 × 50 cm grid.

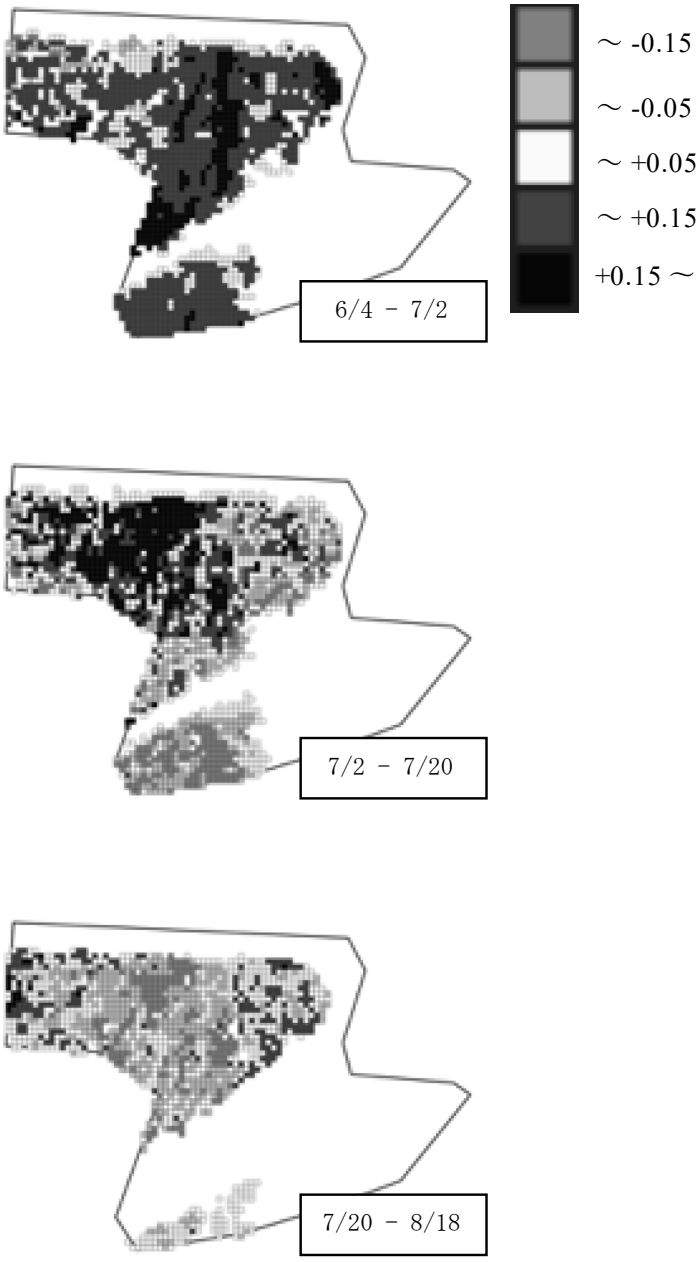

Fig. 2-7

Transition of growth rate (d^{-1}) of the estimated leaf area index (LAI) in each 50 × 50 cm grid.

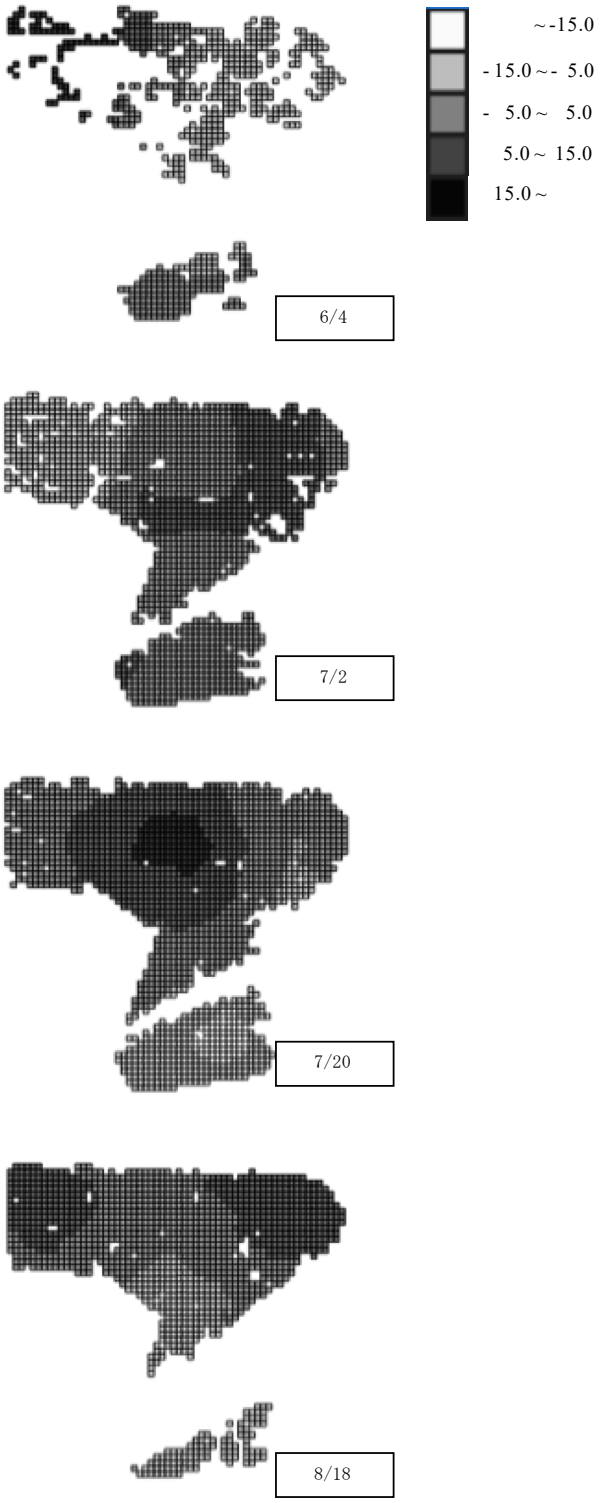

Fig. 2-8

Transition of Getis-Ord Gi* of the estimated leaf area index (LAI) in each 50 × 50 cm grid.

Chapter 3

Analysis of the kudzu community dynamics via aerial image processing and hidden Markov model

Abstract

Modeling of the spatial dynamics of weed communities based on unmanned aerial vehicle (UAV) imagery can contribute to evaluating the probability of occupancy with temporally and spatially high resolution. The Hidden Markov model seemed to be suitable to describe the transition of spatial occupancy because it can be modified flexibly and can include the probability of classification error explicitly. This study aimed to infer the parameters of the kudzu community dynamics and to evaluate its expansion after mowing through aerial image classification and site occupancy model. We obtained the aerial images of the community at the riverbank and identified the grids (0.25 m^2) occupied by kudzu with supervised classification. The hierarchical model comprised the uncertainty of the classification and the transition of the occupancy state of each grid. The posterior distribution of the parameters inferred with Markov chain Monte Carlo methods indicated that the expansion rate after mowing in July was relatively higher than that after mowing in August, suggesting that the compensation for mowing damage is relatively difficult after August, mainly because of small amounts of carbohydrate in storage organs. Combination of image classification and hierarchical modeling would enable us to simulate weed community dynamics on a management scale and to optimize the allocation of resources to reduce the impact of widespread invasive weeds.

Keywords

community dynamics, hidden Markov model, kudzu, remote sensing, supervised classification

Introduction

As demonstrated in Chapter 2, UAV imagery with temporally and spatially high-resolution data is suitable for the evaluation of kudzu community dynamics. The colonization kernel was useful for the estimation of the margin's expansion rate, but the emergence of shoots from the residual organs and the expansion of shoots from the surrounding grids were not divided. Community dynamics consist of different processes, such as emergence, extinction, expansion, and seed dispersal. The hierarchical model accounting for these factors separately and explicitly enables us to evaluate the ecological traits of kudzu spatially and temporally using UAV imagery.

In addition, imagery classification is error-prone, whether manual or automatic, and the understory is also not visible via UAV. Simulation without accounting for misclassification has been known to deviate from the actual phenomena (Royle and Link 2006, Veran *et al.* 2012, Miller et al. 2012, Ferguson *et al.* 2015). Therefore, the transition of latent states and observation processes should be described separately, and the detection probability should be incorporated explicitly into the hierarchical model to estimate real occupancy state stochastically.

The HMM has been applied to many ecological studies (McClintock *et al*. 2020) and seems to be suitable for the estimation of weed community dynamics based on UAV image classification. HMM consists of two models. One of them is a system model, representing time-series transitions of the latent state. In HMM, the conditional probability distribution of future latent states depends only upon the present states. This is called Markov property. The other is an observation model, representing observations conditional on the latent state. Detection probabilities can be incorporated explicitly as parameters in an observation model. This model can be applied in situations in which a site's occupancy state may change through local events, such as emergence, extinction, and colonization. It can be modified flexibly to various ecological problems and seems to be suitable for analyzing plant population dynamics based on time-series spatial data by remote sensing. Posterior distributions of parameters incorporated in complicated hierarchical models can be estimated with Bayesian analysis using Markov chain Monte Carlo (MCMC) methods. MCMC methods consist of algorithms for sampling from a probability distribution and enable to infer parameters in complicated hierarchical models. The hierarchical Bayesian model has been applied to describe populations' spatial dynamics (e.g., Pagel and Schurr 2012, Asada *et al*. 2014, Louvrier *et al*. 2018).

In HMM, the factors on community dynamics are incorporated as probabilities and each process is described stochastically. In Chapter 2, the colonization kernel was applied to evaluate the rate of margins' expansion. The concept of 'colonization' includes the movement and survival which make the colonizers visible in the next observation. In contrast, the kernel in this chapter represents only the movement to adjacent grids in the hierarchical model. Many functions have been proposed as dispersal kernels for plants (Nathan *et al*. 2012), but most of them deal with the dispersal of seed or pollen. The probability of vine expansion has not been examined enough.

The purpose of this chapter is to propose a framework for the evaluation of weed community dynamics by aerial image classification and HMM. A model based on spatially and temporally high-resolution monitoring data of real communities should be constructed to simulate kudzu community dynamics. It is important to explore the optimal timing to mow for the prevention of expansion, based on the quantitative evaluation of ecological traits in each period of the growth. The parameters of the model were inferred from each site's occupancy state classified on the aerial images by machine learning. Based on the posterior distributions of parameters in each period, the effect of the timing of mowing on the emergence and expansion of the community was quantified. In this chapter, the effect was evaluated by comparing spatial dynamics of the communities after mowing in two different timing.

Materials and Methods

Data collection

The experiment was conducted at the bank of the Tenryu River in Higashi-Haruchika, Ina City, Nagano Prefecture (Fig 3-1). The experimental field (35.785 °N, 137.957 °E, 20 m × 80 m) was dominated by kudzu and also grew Japanese mugwort (*Artemisia princeps* Pampan), eulalia grass (*Miscanthus sinensis* Andersson), and black locust (*Robinia pseudoacacia* L.). Two kinds of plots with different management were set up (Fig. 3-2). One was mowed once using a bush cutter with resin cord on July 25, and the other was mowed once on August 25. These plots (5 m in width) were arranged in the north-south direction at 3 m intervals with 3 replications.

The aerial images were obtained from an altitude of 25 m by Phantom 4 (DJI) (spatial resolution: 1.09 cm/pixel) at approximately one-week intervals after each mowing. The

frights were controlled by Pix4Dcaptutre (Pix4D). The orthomosaic images at each observation were generated by Pix4Dmapper (Pix4D). Five ground control points (GCPs) were set in the experimental field, and their coordinates were measured by REACH RS+ (Emlid). The images were divided into regular hexagon grids (0.25 m^2) in ArcGIS Pro (Esri). As described in Chapter 2, I adopted square grids for the quantitation of community expansion and growth. A square grid is surrounded by 8 grids, but the distances to 4 of them is approximately 1.4 times the distances to the others. In this chapter, colonization was evaluated in a shorter span, and the difference made it difficult to evaluate colonization probability impartially regardless of direction. In contrast to a square grid, a hexagon grid is surrounded by 6 grids, and the distance from each to the other is uniform. Each grid was classified to be occupied or not by support vector machine (SVM) based on the brightness of each color band (red, green, blue) of the image. The `ksvm` function in the `kernlab` package (Karatzoglou *et al*. 2004) of R ver. 3.6.0 (R Core Team 2019) was used, the classifiers were trained by the result of manual classification, and the brightness of the 50 grids was selected randomly. The grids were classified into three classes (kudzu, the other plants, and ground) and a linear classifier was applied instead of variable conversion. The result of the classification by SVM was evaluated by comparing them with the result of the manual classification of the other 50 grids selected randomly.

Simultaneously, the images of the area after mowing were recorded by time-laspe camera (Garden Watch Cam, Brinno, Taipei) in Plot C at 1-h intervals for approximately one month after each mowing.

HMM for evaluation of community dynamics

The HMM was applied to evaluate the influence of the timing of mowing on the community dynamics based on the posterior distribution of the parameters. The model consisted of the observation model and the system model. Fig. 3-3 expresses the structure of the hierarchical model.

The observation model expresses the uncertainty of the classification. $z[i,t]$ and $o[i,t]$ $(z[i,t],\ y[i,t] \in 0,1)$ were defined as the true occupancy state and the state classified by SVM at grid i at time t, respectively, having possible states "occupied (1)" or "not occupied (0)". $o[i,t]$ is assumed to follow Bernoulli distribution and can be expressed for $t = 1, \ldots, T$ as

$$o[i,t] \sim Bernoulli(z[i,t]p_{TP}[t] + (1 - z[i,t])p_{FP}[t])$$

where $p_{TP}[t]$ and $p_{FP}[t]$ is the probability of true positive (classifying presence as presence) and false positive (classifying absence as presence) at time t, respectively.

The system model expresses the time-series transitions of the true occupancy state of each gird. For $t = 1$, the occupancy state is expressed as

$$z[i,1] \sim Bernoulli(z_0[i] + (1 - z_0[i])\gamma[i,1])$$

where $z_0[i]$ is the occupancy state just after mowing, classified manually.

The transition of the occupancy state is expressed for $t = 2, \ldots, T$ as

$$z[i,t] \sim Bernoulli(z[i,t-1] + (1 - z[i,t-1])\gamma[i,t])$$

where $\gamma[i,t]$ is the probability that grid i is newly occupied by kudzu between two successive observation periods $t-1$ and t.

$\gamma[i,t]$ is defined as

$$\gamma[i,t] = 1 - (1 - e[t]) \prod_j (1 - c[i,j,t])$$

where $e[t]$ is the probability of emergence and $c[i,j,t]$ is the probability of colonization from grid j to grid i. The event that the grid becomes newly occupied is the complement of the event that neither emergence nor colonization occurs.

$c[i,j,t]$ is defined for $i \neq j$ as

$$c[i,j,t] = \frac{z[j,t]}{\exp(-a[t]\, r[i,j])}$$

where $a[t]$ is the regression coefficient and $r[i,j]$ is the distance between the centroids of the grid i and j. $c[i,j,t]$ is regarded as 0 when $r[i,j] > 3$.

$D_{0.5}/d\,[t]$, an indicator of the rate of expansion, is calculated as

$$D_{0.5}/d\,[t] = -\frac{log(0.5)}{a[t]\;d[t]}$$

$D_{0.5}$ means the distance at which $c[i,j,t]$ becomes 0.5. The quotient divided by the number of days in the period, $d[t]$, was calculated in this study to exclude the effect of the period between observations.

Table 3-1 shows the definition and the prior distribution of parameters incorporated in the model. $e[t]$, $a[t]$, and $D_{0.5}/d\,[t]$ reflect the temporal traits of community dynamics.

Bayesian analysis

The calculation by the MCMC method was executed by JAGS 4.3.0 (Plummer 2003) (Appendix 1) using the `run.jags` function of the `runjags` package (Denwood 2016) of **R** (Appendix 2). The number of chains was assigned to be 3. The numbers of the iterations, the burn-in periods, and the thinning intervals were 1000, 100, and 5, respectively. The trace plots of the parameters were visualized with the `traceplot` function in the `R2jags` package (Su and Yajima 2015).

The convergence diagnosis was based on the trace plots and the Gelman-Rubin statistics ($\hat{R}$) (Gelman and Rubin 1992) of the deviance and the parameters on the temporal trait of community dynamics, $e[t]$, $k[t]$, and $l[t]$. When the trace plots are stable and $\hat{R} < 1.1$, the chains are regarded to be converged.

Results

Classification by SVM

Table 3-2 shows the result of the classification of kudzu's occupancy by SVM. The ratio of true positive and false positive ranged from 0.800 to 1.000 and from 0.143 to 0.750, respectively.

Convergence diagnosis

The trace plots of the deviance, $e[t]$ and $a[t]$, seemed to be mixed and stable (Fig. 3-4). The Gelman-Rubin statistics of the parameters were less than 1.1 (Table 3-3). Consequently, it was confirmed that the chains of each parameter converged.

Interpretation of the posterior distribution

Table 3-3 shows the posterior distributions of the parameters after MCMC sampling. The 95% credible intervals for $p_{TP}[t]$ and $p_{FP}[t]$ were (0.750, 1.000) and (0.000, 0.585), respectively. These intervals did not necessarily include the ratio of true positive and false positive in classification by SVM but were close. The posterior distributions of $e[t]$ did not show significant difference between mowing dates but showed temporal differences after mowing. $e[1]$ and $e[2]$ were nearly 0 regardless of the mowing date. managements. In contrast, the 95% credible intervals for $e[3]$ in the two managements were (0.001, 0.589) and (0.010, 0.614), respectively, indicating that the probability of emergence ranged widely. The posterior distributions of $D_{0.5}/d\,[t]$ were different between mowing dates. $D_{0.5}/d\,[1]$ after mowing in July was relatively lower than that of August, but $D_{0.5}/d\,[2]$ and $D_{0.5}/d\,[3]$ after mowing in July were higher than that of August. These results indicate that the rate of expansion after mowing in July was relatively faster than that after mowing in August.

Fig. 3-5 shows the emergence and expansion of the kudzu shoots after mowing, captured by a time-lapse camera. The shoots started to emerge 3-5 days after mowing. In addition, the expansion of the stems from the buffer area after mowing in July was seemingly faster than that after mowing in August.

Discussion

The 95% credible intervals for the posterior distribution of $p_{TP}[t]$ and $p_{FP}[t]$ (Table 3-3) did not necessarily include the ratio of true positive and false positive in classification by SVM (Table 3-2). The differences between the results of supervised classification and the posterior distributions do not indicate invalidity of the modeling because even manual classification of the training data may have errors. These intervals did not necessarily include the ratio of true positive and false positive in classification by SVM but were close, suggesting that the estimation of the classification processes was reasonable.

$e[1]$ and $e[2]$ was nearly 0 in both the management but $e[3]$ increased and was not significantly different between the managements. The low values of $e[1]$ and $e[2]$ indicate that few new shoots emerged in the two weeks after mowing. Almost all stems from overwintering stems emerge from April to June (Tsugawa et al. 1987); the emergence may be promoted by damage.

The expansion rate, indicated by $D_{0.5}/d\,[t]$, increased in the two weeks after mowing in July and declined in August. The recordings showed that the plot mowed in July was covered with stems growing from the margins in approximately a month while shoot expansion was relatively slow in the plot mowed in August (Fig. 3-6). This indicates that it is relatively hard for kudzu to compensate for mowing damage after August. Carbohydrate is transported to storage organs after September (Rashid et al. 2017). As discussed in Chapter 2, kudzu expands the area in which new stems emerge in the next season through the expansion of stems and transportation of photosynthetic products to the margin of the community during midsummer. Therefore, mowing in August is effective in reducing both the occupied area and the biomass of roots at the margin of the community. The difference in the expansion rates seems to be because of the order of branches, as the expansion of stems depends on higher-order branches after midsummer (Tsugawa and Kayama 1981b). Growth in higher-order branches slows the horizontal expansion rate of the community after August than that after July. In this chapter, I proposed effective means for kudzu community containment based on the community dynamics for three weeks after mowing. To confirm long-term effect on community, it is required to monitor the same community for several years. The model of long-term kudzu community dynamics should include the state of storage organs as a latent state behind the occupancy state or the growth of the aboveground organ.

Describing ecological traits and reaction to the management of each weed species from the viewpoint of spatial dynamics should be applied to evaluate colonization and competition between species. A hierarchical model should be adjusted to the object, and this model still has some room for improvement. In this model, the non-informative prior distributions of the parameters were adopted (Table 3-1). Introducing weakly informative prior distribution based on the results of image classification may help estimate the parameters more practically. For example, the probability distribution of the detection probabilities, $p_{TP}[t]$ and $p_{FP}[t]$, could be estimated from the result of the classifications. There is also a possibility that the small shoots, soon after emergence, could not be detected on the aerial images. According to the recordings, the shoots started to emerge 3-5 days from mowing but they were very thin and tiny (Fig. 3-6). For detecting such tiny shoots, improvement of the quality of image classification, with a smaller size of grids and robust algorithm, is needed.

It may be effective to categorize the growth stage of shoots in each grid for the

detection of tiny shoots at early growth stages. Incorporating transition probability among growth stages can also prove to be effective. Muranaka and Washitani (2003) applied the transition matrix of the growth stage and colonization probability to the population model of weeping lovegrass (*Eragrostis curvula* (Schrad.) Nees.). The probability of death should also be incorporated into the model for the examination of community dynamics throughout the season.

In this study, the parameters on emergence and colonization were defined to depend only on time but they should also include spatial factors, such as spatial autocorrelation. In particular, the posterior distribution of $e[3]$ ranged widely in both the management. Incorporating spatial factors explicitly in the hierarchical prior distribution (Lamiter et al. 2006) may be useful in the evaluation of ecological traits and the precise prediction of community dynamics. Spatial factors reflect the morphological features and propagation strategy of each weed species or population. Rooted nodes of kudzu decrease, and their spatial distribution becomes more uniform as they become older (Tsugawa and Kayama 1974, Tsugawa and Kayama 1975, Tsugawa and Kayama 1978). Understanding the spatial heterogeneity of emergence will reflect the background of a population.

In addition, the probabilities of colonization were calculated for all the other grids for the generalization of the model. Consequently, the calculation load was very heavy. The colonization in only the nearby grids should be considered for modeling. The distance to consider should be adjusted according to the rate of the spread and the frequency of observations. The colonization kernel function should be examined further based on the morphology of vines. In this model, the probability of vine expansion was regarded to decline with increasing distance from the source grid. Using data with higher spatial resolution, the colonization kernel can be inferred more precisely.

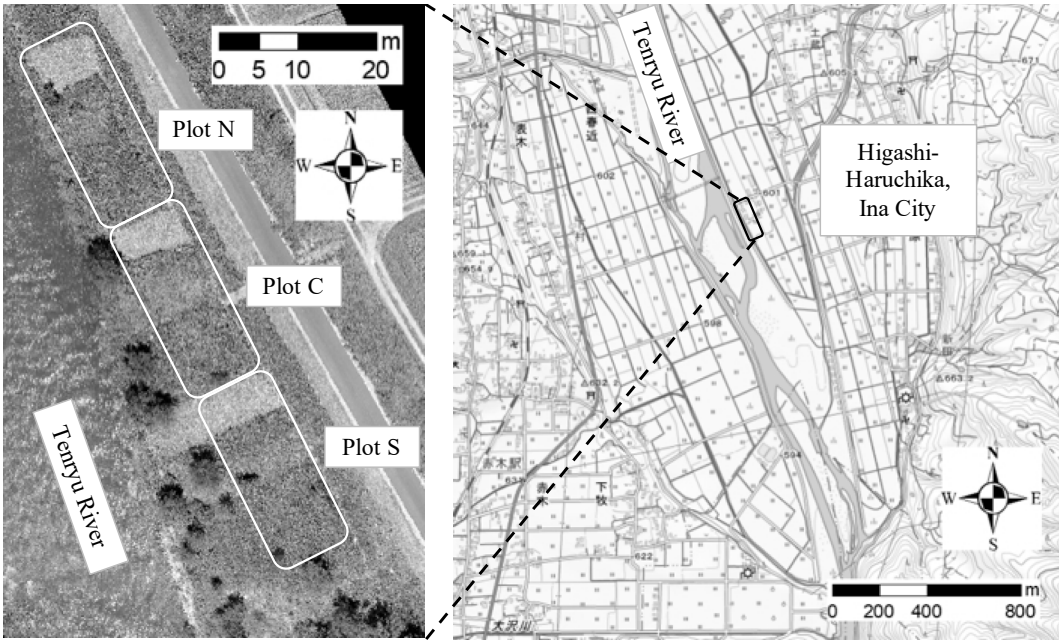

Fig. 3-1

Location of the experimental areas.

The aerial image (left) was obtained soon after mowing on August 25.

The map (right) is based on a digital map published by the Geospatial Information Authority of Japan.

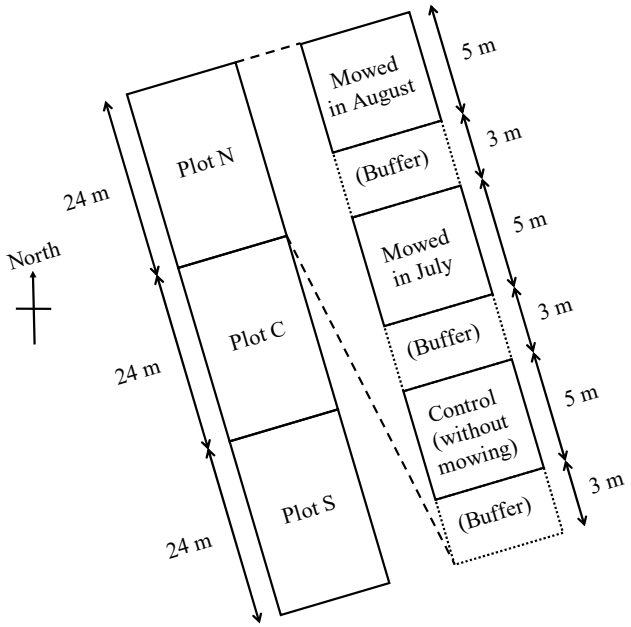

Fig. 3-2

Arrangement of the experimental plots.

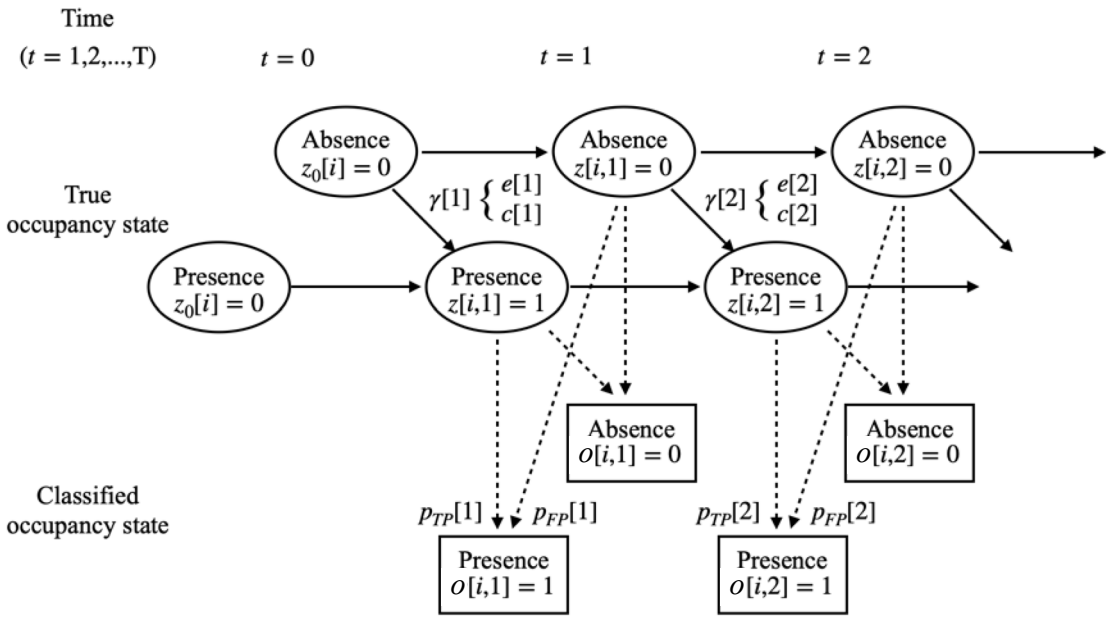

Fig. 3-3

The structure of the hidden Markov model (HMM) describing transition of occupancy state in each hexagon grid.

Table 3-1

The parameters in the model to be estimated.

The prior distribution and the initials were common to both the managements.

Variable	Prior distribution	Initial	
p_{TP}	beta(1, 1)	0.5	Probability of true positive
p_{FP}	beta(1, 1)	0.5	Probability of false positive
e	beta(1, 1)	0.5	Probability of emergence
a	uniform(0, 10)	1.0	Regression coefficients of the colonization kernel

Table 3-2

The result of the image classification of kudzu's occupancy by support vector machine (SVM).

Mowing on 7/25

t = 1 (8/2)

		Classification by SVM +	-
Manual classification	+	12	3
	-	5	30
The ratio of true positive:			0.80
The ratio of false positive:			0.14

t = 2 (8/9)

		Classification by SVM +	-
Manual classification	+	19	2
	-	9	20
The ratio of true positive:			0.90
The ratio of false positive:			0.31

t = 3 (8/17)

		Classification by SVM +	-
Manual classification	+	32	2
	-	10	6
The ratio of true positive:			0.94
The ratio of false positive:			0.63

Mowing on 8/25

t = 1 (8/31)

		Classification by SVM +	-
Manual classification	+	18	0
	-	6	26
The ratio of true positive:			1.00
The ratio of false positive:			0.19

t = 2 (9/9)

		Classification by SVM +	-
Manual classification	+	17	4
	-	8	21
The ratio of true positive:			0.81
The ratio of false positive:			0.28

t = 3 (9/18)

		Classification by SVM +	-
Manual classification	+	38	0
	-	9	3
The ratio of true positive:			1.00
The ratio of false positive:			0.75

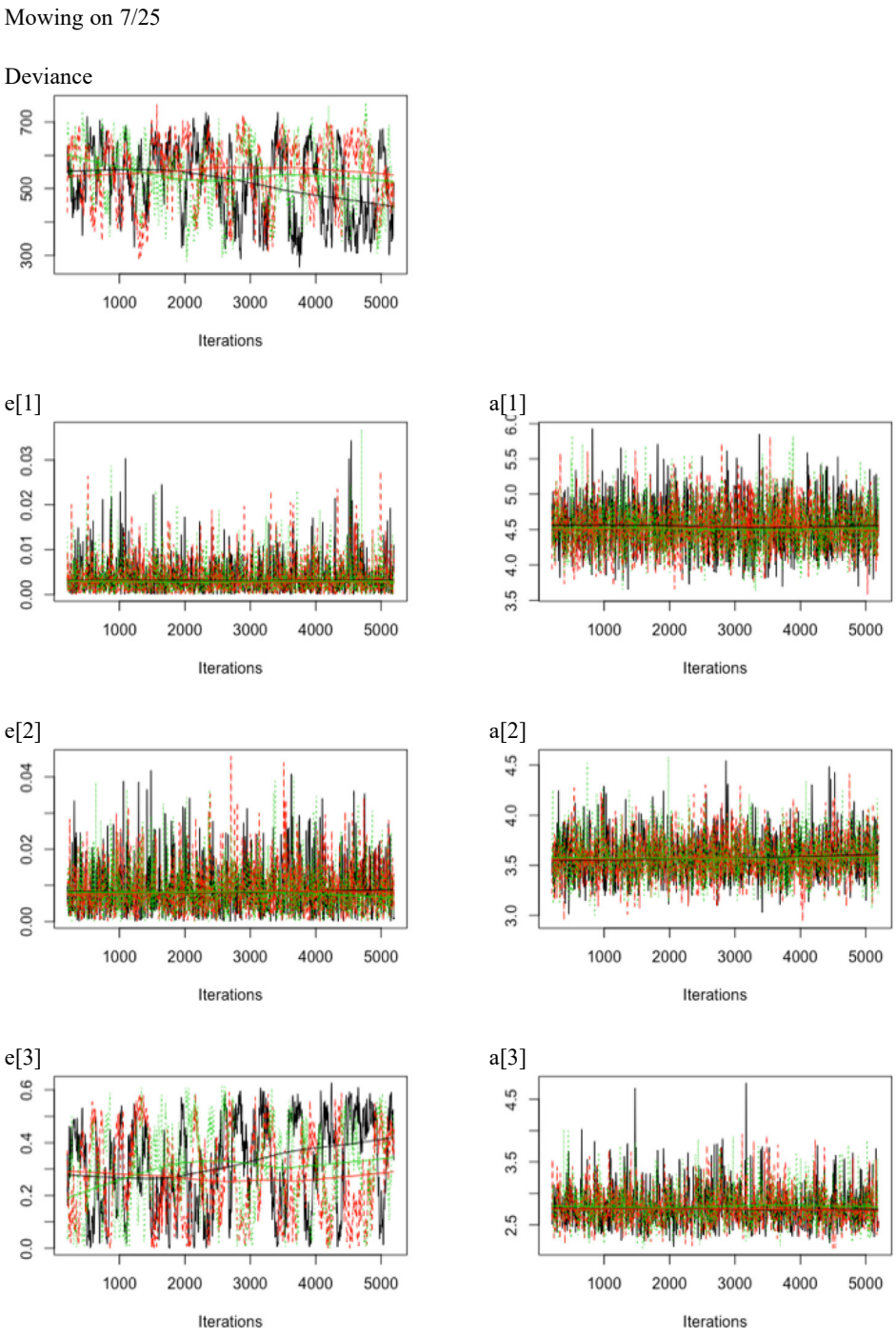

Fig. 3-4

The trace plots of the deviance, $e[t]$ and $a[t]$ drawn with `traceplot` functions in `R2jags` package in the models describing kudzu community dynamics after mowing. Each line presents the trace plot of each chain in the calculation.

Mowing on 8/25

Deviance

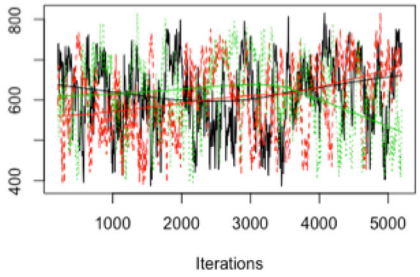

e[1]

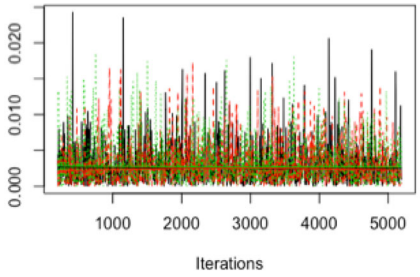

a[1]

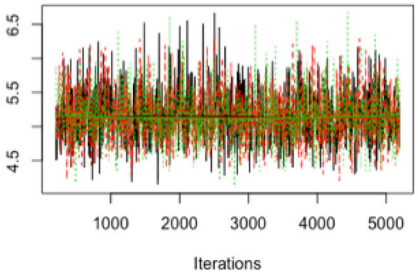

e[2]

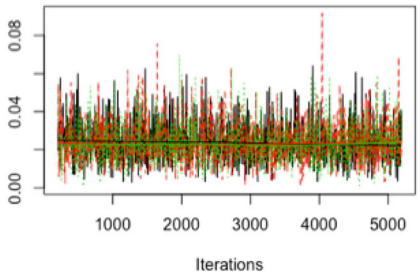

a[2]

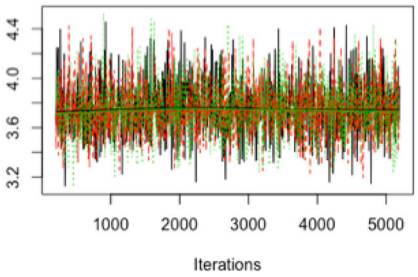

e[3]

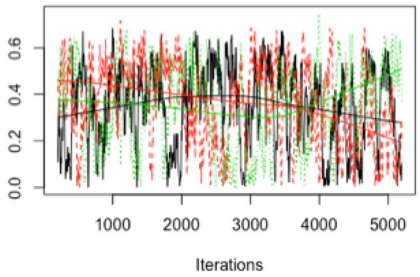

a[3]

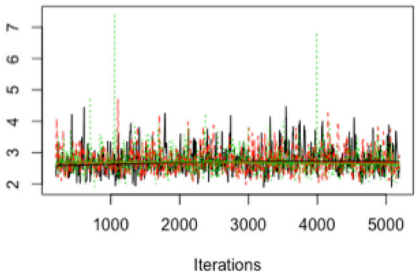

Fig. 3-4 (continued)

Table 3-3

Gelman-Rubin statistics and posterior distribution of the deviance and the parameters. SD and q_x mean the standard deviance and the 100x th percentile of the posterior probability distribution, respectively.

Mowing on 7/25

Parameter	Gelman-Rubin staticstics	Mean	SD	$q_{0.025}$	$q_{0.500}$	$q_{0.975}$
Deviance	1.019	534.927	99.140	342.421	547.901	692.163
p_{TP}[1]	1.000	0.802	0.026	0.750	0.803	0.851
p_{TP}[2]	1.001	0.996	0.004	0.989	0.997	1.000
p_{TP}[3]	1.000	0.997	0.003	0.991	0.998	1.000
p_{FP}[1]	1.002	0.003	0.003	0.000	0.002	0.009
p_{FP}[2]	1.003	0.012	0.007	0.000	0.011	0.027
p_{FP}[3]	1.019	0.326	0.159	0.019	0.345	0.562
e[1]	1.006	0.004	0.004	0.000	0.003	0.012
e[2]	1.002	0.009	0.007	0.000	0.007	0.023
e[3]	1.016	0.295	0.163	0.001	0.302	0.539
a[1]	1.001	4.541	0.348	3.895	4.519	5.209
a[2]	1.000	3.583	0.222	3.169	3.568	4.020
a[3]	1.004	2.795	0.306	2.282	2.755	3.436
$D_{0.5}$/d[1]	1.001	0.022	0.002	0.019	0.022	0.025
$D_{0.5}$/d[2]	1.000	0.028	0.002	0.024	0.028	0.031
$D_{0.5}$/d[3]	1.003	0.031	0.003	0.025	0.031	0.038

Mowing on 8/25

Parameter	Gelman-Rubin staticstics	Mean	SD	$q_{0.025}$	$q_{0.500}$	$q_{0.975}$
Deviance	1.002	609.433	90.016	433.275	616.679	755.494
p_{TP}[1]	1.000	0.968	0.010	0.948	0.969	0.986
p_{TP}[2]	1.001	0.920	0.015	0.890	0.921	0.949
p_{TP}[3]	1.000	0.979	0.007	0.964	0.980	0.992
p_{FP}[1]	1.003	0.003	0.003	0.000	0.002	0.009
p_{FP}[2]	1.000	0.005	0.005	0.000	0.003	0.015
p_{FP}[3]	1.002	0.321	0.176	0.001	0.328	0.585
e[1]	1.000	0.003	0.003	0.000	0.002	0.009
e[2]	1.001	0.024	0.011	0.003	0.023	0.045
e[3]	1.001	0.354	0.177	0.010	0.379	0.615
a[1]	1.000	5.152	0.382	4.456	5.130	5.950
a[2]	1.000	3.748	0.216	3.331	3.735	4.178
a[3]	1.002	2.732	0.399	2.014	2.674	3.460
$D_{0.5}$/d[1]	1.000	0.027	0.002	0.023	0.027	0.031
$D_{0.5}$/d[2]	1.000	0.021	0.001	0.018	0.021	0.023
$D_{0.5}$/d[3]	1.001	0.029	0.004	0.021	0.029	0.036

Mowing on 7/25

7/27 (2 days after mowing)

8/3 (1 week after mowing)

8/10 (2 weeks after mowing)

8/17 (3 weeks after mowing)

Fig. 3-5

Emergence and expansion of kudzu shoots after mowing captured by time-laspe camera (Garden Watch Cam, Brinno, Taipei).

The images were taken in the south of Plot C.

Mowing on 8/25

8/26 (1 day after mowing)

9/3 (1 week after mowing)

9/10 (2 weeks after mowing)

9/17 (3 weeks after mowing)

Fig. 3-5 (continued)

Chapter 4

Influence of leaf orientation movements on light interception and the photosynthetic reaction of kudzu canopy

Abstract

Leaf orientation of kudzu plays a key role in avoiding light and heat; however, the effect of light penetration on the photosynthetic efficiency of a whole canopy has not been investigated. This study aimed to evaluate the effect of leaf orientation on light interception and the photosynthetic efficiency of kudzu canopies in the field. The light acclimation mechanisms of the kudzu canopy were revealed by evaluating the environmental and photosynthetic parameters using a portable spectrophotometer for rapid measurement. Paraheliotropic movement helped the uppermost leaves avoid intense direct solar radiation and increased light penetration into the canopy. The linear electron flow in the lower leaves increased while that at the surface did not considerably decrease from the light-saturated values, suggesting that photosynthetic efficiency of a whole canopy improved by light penetration. The lower leaves exposed to intense light dissipated excess energy with non-photochemical quenching. These findings indicate that the adaptive function of leaf orientation involves maximizing the photosynthetic efficiency in the whole canopy while avoiding photoinhibition in individual leaves on the surface.

Keywords: kudzu, leaf orientation, light penetration, photoinhibition, photosynthetic efficiency

Abbreviations

CEF – cyclic electron flow

ECS – electrochromic shift

Fv'/Fm' – quantum yield of open photosystem II

LAI – leaf area index

LEF – linear electron flow

NPQ – non-photochemical quenching

νH^+ - steady-state proton flux

PAM – pulse amplitude modulation

PAR – photosynthetic active radiation

Φ_{NPQ} – quantum yield of NPQ in photosystem II

Φ_{II} – quantum yield of photochemical reaction in photosystem II

pmf – proton motive force

q_P – fraction of open reaction center in photosystem II

Introduction

Kudzu has been known for its leaf orientation and its effects on solar radiation, and the water use efficiency of an individual leaf has been investigated (Forseth and Teramura 1986, Liu *et al*. 1997a, Liu *et al*. 1997b). However, the effect of kudzu canopy as a whole on light condition and photosynthetic efficiency has not been investigated. That requires the measurement of solar radiation at different depths of the kudzu canopy in the field.

Cotton (*Gossypium hirsutum* L.), sunflower (*Helianthus annuus* L.), black pine (*Pinus thunbergii* Parl.), and some legumes are also known for their leaf orientation (Kawashima 1969, Lang 1973, Wien and Wallace 1973, Shell *et al*. 1974, Tashima *et al*. 2004, Xu *et al*. 2009). The leaf orientation in the uppermost layer of the dense peanut (*Arachis hypogaea* L.) canopy decreases radiation intercepted in the uppermost layers and increases in the lower layers (Isoda *et al*. 1993a). The effect of leaf orientation on radiation interception in the soybean (*Glycine max* Merr.) canopy depends on cultivars (Isoda *et al*. 1993b), and cultivars with low transpiration ability have active paraheliotropism (Isoda *et al*. 1996).

Light penetration has been discussed as a primary factor in the radiation use efficiency of canopies (Monteith 1977, Sinclair *et al*. 1992). Paraheliotropism might raise photosynthetic efficiency through improvement in light penetration. At the same time, lower leaves become exposed to sunflecks—intense and fluctuating direct radiation. Leaf acclimates to light conditions through growth, but rapid changes in light intensity do not allow the leaf to adopt the corresponding photosynthetic function quickly. A leaf exposed to intense radiation dissipates excess energy as fluorescence and heat, through a physiological process called quenching. Heat dissipation (non-photochemical quenching; NPQ) is a photoprotective mechanism and is thought to be enhanced by xanthophyll deep oxidation, which is activated by the transthylakoid proton motive force (*pmf*) (Kramer *et al*. 1999). The lower leaves of kudzu are suspected to adapt to the prevailing light conditions through improving their efficiency of NPQ and/or activating cyclic electron flow (CEF).

Chlorophyll fluorescence measurement by pulse amplitude modulation (PAM) fluorometry is widely utilized to evaluate photosynthetic activity under various environmental and physiological conditions. Horizontally held leaves of a tropical pioneer tree (*Macaranga conifera* (Zoll.) Műll.Arg.) exhibited higher photosystem II

quantum yield (Φ_{II}) at dusk than just before dawn (Ishida *et al*. 1999). Xu *et al*. (2009) measured the chlorophyll fluorescence of shade-adapted black locust (*Robinia pseudoacacia* L.) grown in a pot and reported that photoinhibition in excessive light in water-stressed plants was lower than that in well-watered plants and this plasticity to the environment might contribute to better survival in the understory. Although the effects of leaf movement on the photosynthetic activity of leaves have been investigated in previous studies, the effect of light penetration on the photosynthetic activity of the canopy is still obscure. An increase in penetrating radiation can promote photosynthesis and photodamage, simultaneously. To understand the photosynthetic efficiency of the layered plant canopy, light conditions and photosynthetic activity have to be measured at each level. However, such a comprehensive field study has not been accomplished because of technical difficulties.

This study aimed to evaluate the effects of leaf orientation on the light interception and photosynthetic efficiency of the kudzu canopy in the field. In the treatment plots, leaf movements in the uppermost layer were restrained by a nylon net. The radiation intercepted in each layer of the kudzu canopy was measured using solarimeter films. At the same time, the leaf angle and chlorophyll fluorescence were also measured by a portable device, MultispeQ (Kuhlgert *et al*. 2016). MultispeQ can collect the real-time data of chlorophyll fluorescence and leaf angle in a short time. It has previously been used for field-based evaluation of phenotypic performance (Fernández-Calleja *et al.* 2020) and seemed to be appropriate to monitor photosynthetic activity at the different levels of a plant or canopy. The portable device enabled us to quantify each layer's physiological reactions and was helpful in the evaluation of the photosynthetic efficiency of the canopy as a whole in the field.

Materials and Methods

Experimental design

The experiment was conducted at the bank of the Mibu River, Ina City, Nagano Prefecture (lat. 35° 49' N, long. 137° 58' E) on September 17–19, 2018 (Fig. 4-1). Kudzu's leaf area is the largest in this period of the season (Tsugawa and Kayama 1981a). During our experimentation, the weather was mainly sunny and the sky, overcast with no rainfall. The kudzu formed uniform canopies, and its height was approximately 100 cm.

The treatment plots and the control plots (180 × 180 cm) were arranged alternately in the east-west direction with 3 replicates each (Fig. 4-2). The treatment plots were covered with nylon nets (mesh size: 45 mm) to protect the orientation of the uppermost leaves of the canopies in the evening (after the leaves became horizontal) of 16 September (Fig. 4-3).

Data collection

The intercepted radiation and photosynthetic parameters were measured in the quadrat (50 × 50 cm) set up in the center of each plot (Fig. 4-4). The cumulative horizontal radiation for three days was measured at depths of 0, 20, 40 cm from the surface of the canopy by a solarimeter film (Taisei Fine Chemical Co. Ltd., OptoLeaf R-3D, Chiba) with 3 replicates. The films (20 × 35 mm, 0.1 g) were bound on the rings horizontally in the quadrat in the evening of 16 September and collected in the evening of 19 September. The amount of light quantum [mol photons m^{-2}] was estimated from the degree of color degradation of the film measured by a spectrophotometer (Taisei Fine Chemical Co. Ltd., D-Meter RYO-470, Chiba). The vertical distribution of the LAI was examined by the stratified-clipping method at 20 cm intervals on 20 September. The leaves were scanned and the area of the leaves was measured by Fiji of the imageJ package (Schindelin *et al*. 2012).

The 5 leaflets that were selected to measure the cumulative solar radiation in each quadrat were subjected to multiple measurements by MultispeQ v1.0 device (Kuhlgert *et al*. 2016) at 10–11 AM of every day from September17–19. MultispeQ was developed in the laboratory of David Kramer (Michigan State University, Michigan, USA) and controlled by “Leaf Photosynthesis MultispeQ V1.0” protocol in the “PhotosynQ” open access platform (https://www.photosynq.com). It took approximately 1 min to sample a leaf and two devices were used to reduce sampling time. The object. That is, the leaf was bound by a clamp at the point of the device. The photosynthetic active radiation (PAR) (μmol photons m^{-2} s^{-1}) was measured by a sensor at the top of the device. The radiation was reproduced in the chamber inside the clamp with LED lamps. The leaf angles (0°–90° (horizontal-vertical)) were also measured by the sensor on the device. Clamping the leaf without changing the angle enables real-time measurement of leaf orientation.

MultispeQ also measures chlorophyll fluorescence by PAM techniques in the chamber and calculates the parameters of photosynthetic activity. Linear electron flow

(LEF) is proportional to PAR and photosystem II quantum yield (Φ_{II}) is as the following equation:

$$\mathrm{LEF} = 0.84 \times 0.5 \times \mathrm{PAR} \times \Phi_{\mathrm{II}}$$

Φ_{II} is the product of photochemical quenching (q_P) and quantum yield of open photosystem II (Fv'/Fm'). q_P indicates the fraction of open (ready for photochemical reaction) reaction center in photosystem II, but the value reflects the functions of its downstream components. For roughly estimating the gross primary production of a whole canopy, the LEF was integrated with respect to LAI. In this integration, the leaves at a depth of 0–10 cm (the upper half of the LAI at a depth of 0–20 cm), 10–30 cm (the lower half of the LAI at a depth of 0–20 cm and the upper at 20–40 cm), and 30–40 cm (the lower half of the LAI at a depth of 20–40 cm) were regarded to photosynthesize in the LEF measured at depths of 0, 20, and 40 cm, respectively.

As an indicator of non-photochemical quenching (NPQ), MultispeQ provides a parameter named NPQt, which is proportional to NPQ provided by conventional PAM fluorometers but does not require dark adaptation of a leaf sample (Tietz *et al*. 2017). *pmf* can be detected as an absorbance spectrum shift of membrane-embedded carotenoids (electrochromic shift; ECS). MultispeQ also measures absorbance change around 530 nm during the light-to-dark transition and provides ECS parameters, ECSt, and νH^+, representing the magnitude of *pmf* and proton flux, respectively (Cruz *et al*. 2001).

Statistical analysis

All statistical analyses were done with **R** ver. 3.6.0 (R Core Team 2019). The parameters at each level of the canopy were compared employing Welch's two-sample t-test.

Results

Leaf angle and light interception

The leaf angle (Table 4-1a) at the surface of the canopy in the treatment plots was significantly lower than that in the control plots ($P < 0.01$); it was nearly horizontal. This shows that the nylon net successfully prevented the orientation of the leaves at the surface of the canopy. In contrast, the leaf angle at depths of 20 cm and 40 cm from the surface of the canopy in both plots were not significantly different. The PAR (Table 4-1b) at the surface of the canopy in the treatment plot was 41.0% higher and had a narrower range

than that in the control plot ($P < 0.01$). In contrast, the PAR at a depth of 20 cm in the treatment plot was 70.9% lower and had a narrower range than that in the control plot ($P < 0.01$). Fig. 4-5, showing the relationship between the leaf angle and the PAR, suggests that the treatment exposed the leaves on the surface to intense radiation.

The LAI at a depth of 0–20 cm, 20–40 cm and 0–40 cm (4.7 on average) was not significantly different ($P = 0.652$, 0.100, 0.191, respectively) (Table 4-2). The cumulative horizontal radiation for three days at a depth of 20 cm in the treatment plots was 25.3% lower than that in the control plots but not significantly ($P = 0.362$) (Table 4-1c). The uppermost leaves in the treatment plots seemed to prevent sunlight from penetrating the canopy.

Photosynthetic reaction

The LEF (Fig. 4-6) at a depth of 20 cm in the treatment plot was 59.8% lower and had a narrower range than that in the control plot ($P < 0.01$), while that at the surface in treatment plots was 12.9% higher than that in control plot ($P = 0.054$). There was little difference between the control and treatment plots in the saturation of LEF under intense radiation, but some leaves in the treatment plots showed relatively low LEF (50–150 μmol electrons $m^{-2} s^{-1}$) under high PAR (1000–2000). Fig. 4-7b shows that Φ_{II} declined linearly with increasing light intensity and the trends were not different between the plots, indicating that saturation of LEF was due to lower Φ_{II} under intense radiation. q_P and Fv'/Fm' responded to light intensity in the same way as Φ_{II} (Fig. 4-7c, d). Fig. 4-8 shows the integral of LEF with respect to depth per unit leaf area. The value at a depth of 0–40 cm in the treatment plot was 28.3% lower than that in the control plots ($P = 0.052$). This degradation of productivity seemed to be mainly due to a significant decrease in the depth of 20–40 cm ($P = 0.036$).

Fig. 4-9a shows that NPQt increased linearly with increasing light intensity and the trends are not different between the plots. The ratio of NPQt to LEF was not different between the two plots (Fig. 4-10a). ECSt was saturated under intense radiation (Fig. 4-9b) and was proportional to LEF; the trends were not different between the plots (Fig. 4-10b). NPQt increased in association with ECSt and the trends were not different between the plots (Fig. 4-11). Fig. 4-10c shows that vH^+ was proportion to LEF and the trends were not different between the plots.

Discussion

The leaf orientation at the surface of the canopy allowed sunlight to penetrate the canopy (Table 4-1a). The projected area of the leaves becomes smaller by paraheliotropic movement and the direct radiation could reach the lower leaves. The LAI of the canopy with a thickness of 40 cm (4.7 on average) (Table 4-2a) is equivalent to a densely planted peanut var. Nakateyutaka planted with 20 cm spacing (4.8) (Isoda *et al*. 1993a) or soybean var. Valencia planted with 30 cm spacing (approximately 5.0) (Isoda *et al*. 1996). Kudzu forms a relatively dense canopy in the legumes and therefore, paraheliotropic movement helps uppermost its leaves to avoid intense direct solar radiation and increase irradiance on lower leaves (Table 4-1b).

On the surface of the canopy, the LEF (Fig. 4-6) was elevated by treatment due to stronger light intensity (Fig. 4-7a). The lower leaves showed lower LEF in the treatment plot due to weaker light intensity. This decrease was caused by a decline in qP and Fv'/Fm' (Fig. 4-7b, c, d), indicating that LEF was regulated by both closure and quantum yield of photosystem II. Consequently, the gross primary production of the canopy is improved by light penetration (Fig. 4-8). The increase in LEF on the surface leaves by treatment was less significant than the decrease in LEF on the lower leaves, mainly due to the saturation of LEF under intense radiation. These findings suggest that leaf orientation contributes to maximizing photosynthetic efficiency throughout the canopy. This effect should be regarded as an adaptive function of diurnal leaf movement, as well as for avoiding photoinhibition in individual leaves on the surface. Climbing plants including kudzu have an especially flexible three-dimensional architecture and each leaf receives variable light conditions. The leaves at a lower position of horizontally trained watermelon show higher solar radiation and photosynthetic rate than vertically trained leaves (Watanabe *et al*. 2001). When the canopy grows vertically, leaf orientation would affect light interception and photosynthetic efficiency greatly.

The lower leaves sometimes received intense radiation (Table 4-1b), indicating that they were exposed to sunflecks. As they did not change their angle significantly (Table 4-1a), they needed to dissipate the excess energy. The increase in NPQ under higher light intensity (Fig. 4-9a) indicated that the leaves successfully dissipate excess energy under intense radiation. The contribution of LEF to NPQ does not seem to be changed by leaf orientation (Fig. 4-10a). The transthylakoid proton gradient increases with increasing light intensity and is saturated under intense radiation (Fig. 4-9b). The efficiency of the

xanthophyll cycle did not seem to increase due to sunflecks because the ratio of ECS to NPQ did not change (Fig. 4-11). The ratio of ECS to LEF did not increase due to the treatment (Fig. 4-10b). The contribution of CEF to proton flux did not change due to exposure to sunflecks (Fig. 4-10c). CEF has been suggested to play an important role in maintaining the photosynthetic rate under fluctuating radiation (Yamori et al. 2019), but there was no evidence of CEF activation through light penetration. These results indicate that the lower leaves of the kudzu canopy dissipated excess energy neither by improving the efficiency of the xanthophyll cycle nor CEF but simply with the acceleration of LEF. This suggests that kudzu adopts multiple mechanisms for dealing with intense and fluctuating radiation and has a high potential for adaption to light conditions. Kudzu forms mantle communities on the edge of the forest, which is often exposed to direct solar radiation. In addition, vine species lean on other plants or themselves and acquire highly variable structures. Therefore, the leaves of kudzu adapt flexibly to changing light conditions.

In this study, I only analyzed the short-term influence of leaf orientation to clarify its effects on light interception and photosynthetic efficiency. If the treatment continued for a few weeks or months, less light penetration into the canopy should lead more selective allocation of photosynthetic products and nitrogen to the surface. Nitrogen will be transported from the older leaves inside the canopy to the younger ones on the surface (Field 1983). Leaves to be extended newly on the surface might become thicker than the leaves extended inside the canopy (Boyne et al. 2013). Furthermore, life span of individual leaf might become shorter to concentrate resources younger leaves on the surface constantly (Hikosaka 2003). These allocation of photosynthetic products and nitrogen will maximize photosynthetic efficiency. To investigate the productivity of kudzu canopy, long-term field observation should be required to measure the physiological and morphological traits and the life span of each leaf.

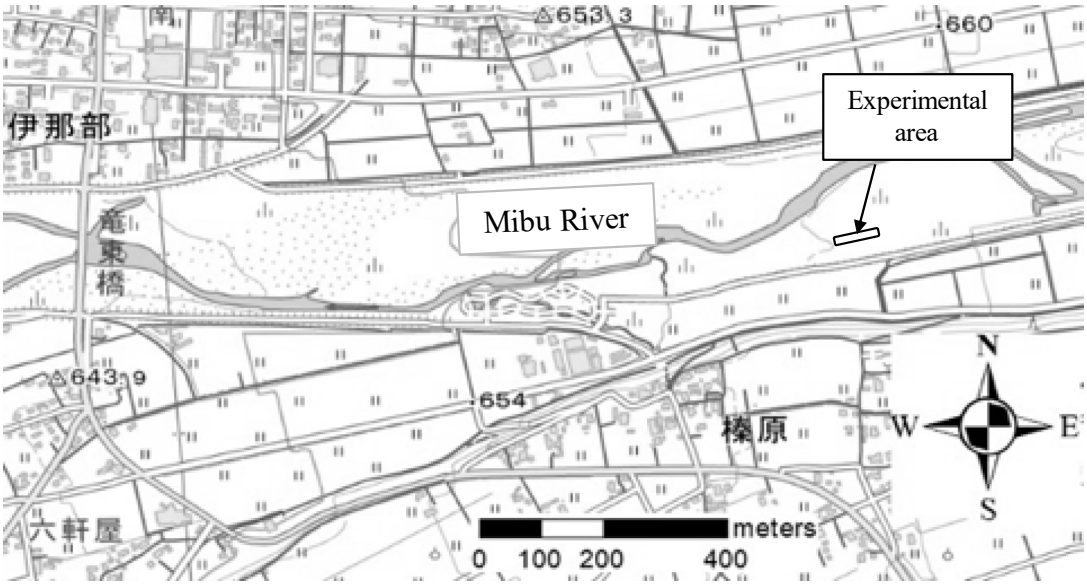

Fig. 4-1

Location of the experimental areas.

This map is based on a digital map published by the Geospatial Information Authority of Japan.

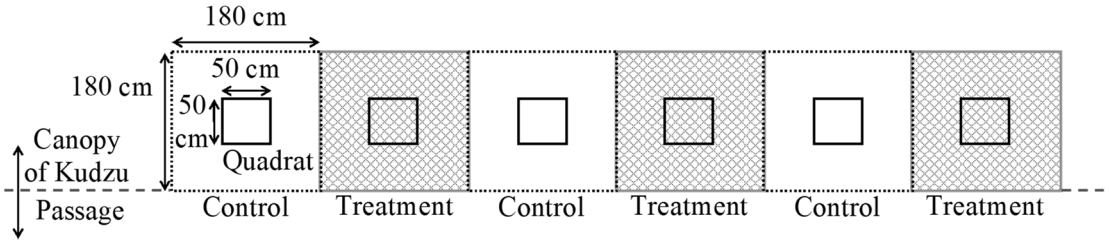

Fig. 4-2

Arrangement of the experimental plots.

The treatment plots and the control plots (180 cm × 180 cm) were located on the passage in the riverbank and arranged alternately. The quadrat was set in the center of each plot.

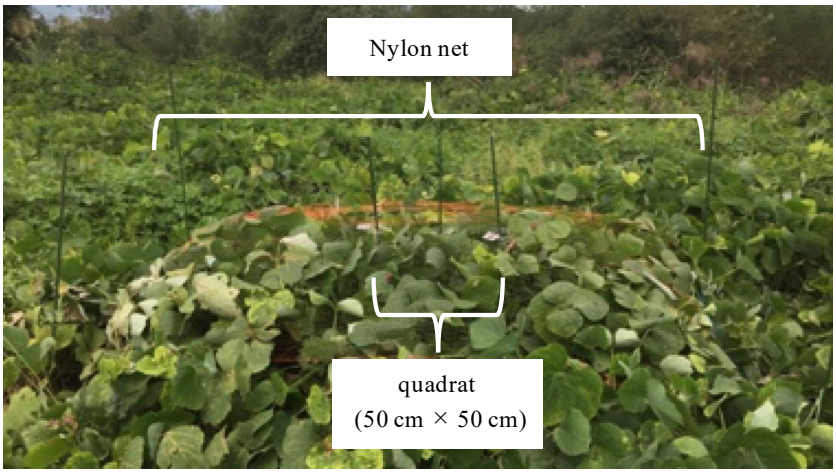

Fig. 4-3

Treatment restricting the leaf orientation of the uppermost leaves.

In the treatment plots, the uppermost leaves were covered with the nylon net. In the quadrat, 3 poles were set for installation of solarimeter film.

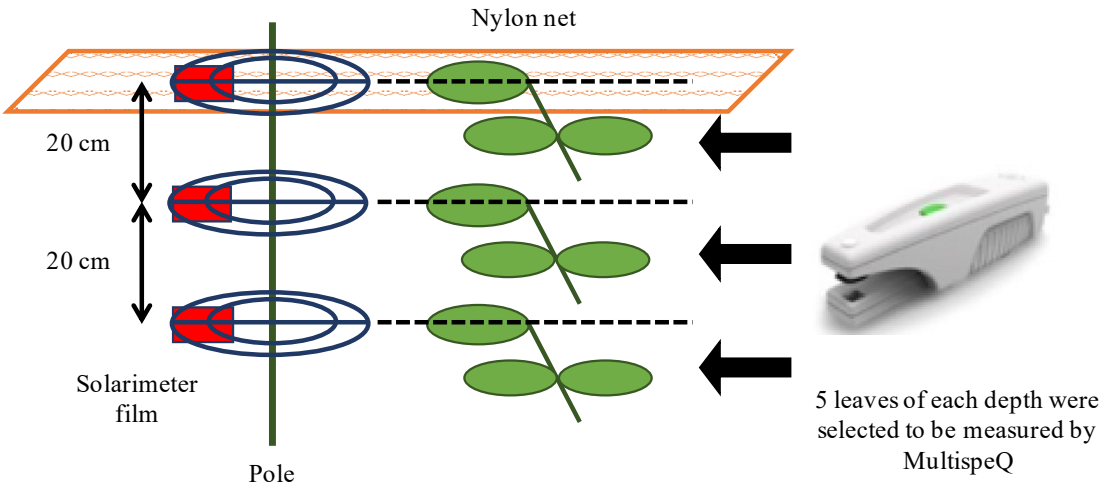

Fig. 4-4

Method for the measurement of radiation and chlorophyll fluorescence in the treatment plot.

The control plot did not have a nylon net setting to protect leaf orientation.

Table 4-1

Leaf angle, photosynthetic active radiation (PAR), and cumulative horizontal radiation at various depths in the kudzu canopy in the control and treatment plots.

The values represent mean ± standard deviation. *P* is the probability that the two plots have equal means, calculated by of Welch's two-sample t-test.

(a) Leaf angle [°]

Depth	Control	Treatment	*P*
0 cm	58.6 ± 28.8	17.2 ± 13.7	< 0.01
20 cm	22.6 ± 17.3	17.7 ± 17.0	0.177
40 cm	17.2 ± 14.0	13.3 ± 11.0	0.142

(b) PAR [μmol m^{-2} s^{-1}]

Depth	Control	Treatment	*P*
0 cm	1055 ± 530	1488 ± 422	< 0.01
20 cm	572 ± 601	166 ± 340	< 0.01
40 cm	70 ± 98	53 ± 31	0.281

(c) Cumulative horizontal radiation [mol m^{-2}]

Depth	Control	Treatment	*P*
0 cm	105.4 ± 9.5	109.6 ± 10.7	0.394
20 cm	33.5 ± 12.6	25.0 ± 23.7	0.362
40 cm	3.8 ± 3.3	3.6 ± 2.8	0.874

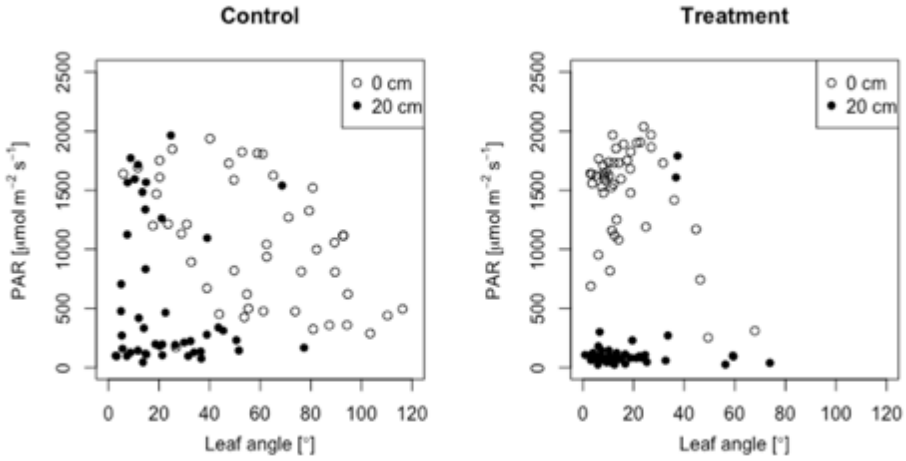

Fig. 4-5

Relationship between leaf angle and photosynthetic active radiation (PAR) at various depths in the kudzu canopy in the control and treatment plot.

Table 4-2

Leaf area index (LAI) of each layer in the kudzu canopy of the control and treatment plots. The values represent mean ± standard deviation. *P* is the probability that the two plots have equal means, calculated by of Welch's two-sample t-test.

Depth	Control	Treatment	*P*
0-20 cm	2.39 ± 0.34	2.56 ± 0.47	0.652
20-40 cm	1.85 ± 0.45	2.54 ± 0.22	0.100
0-40 cm	4.24 ± 0.77	5.09 ± 0.45	0.191

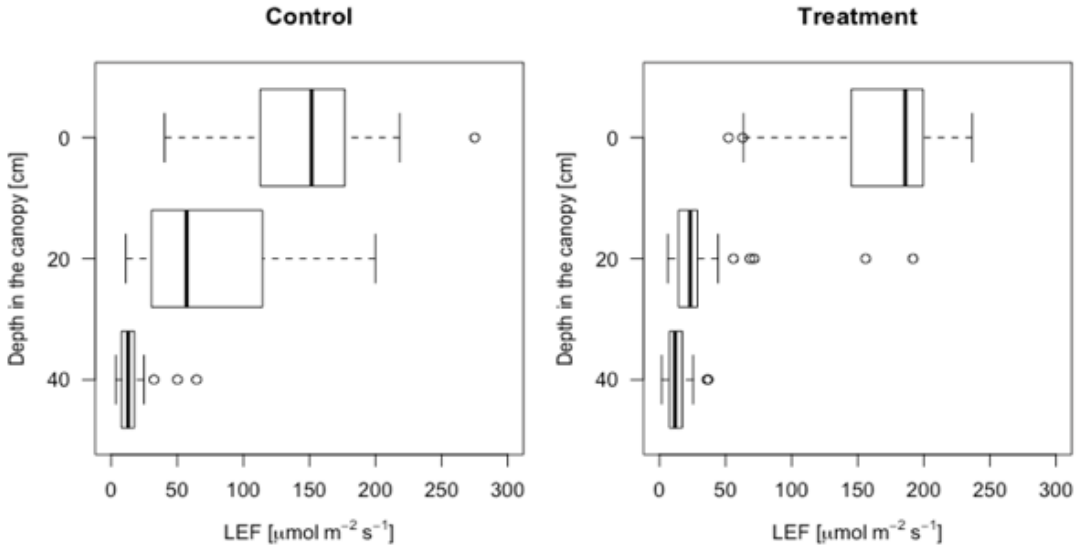

Fig. 4-6

Linear electron flow (LEF) at various depths in the kudzu canopy in the control and treatment plot.

The line in the box indicates the median, the box indicates the first and third quantiles, and the whiskers indicate the highest/lowest value that is within 1.5 times the interquartile range from the box. The outliers indicate the data beyond the end of the whiskers.

(a) LEF vs PAR

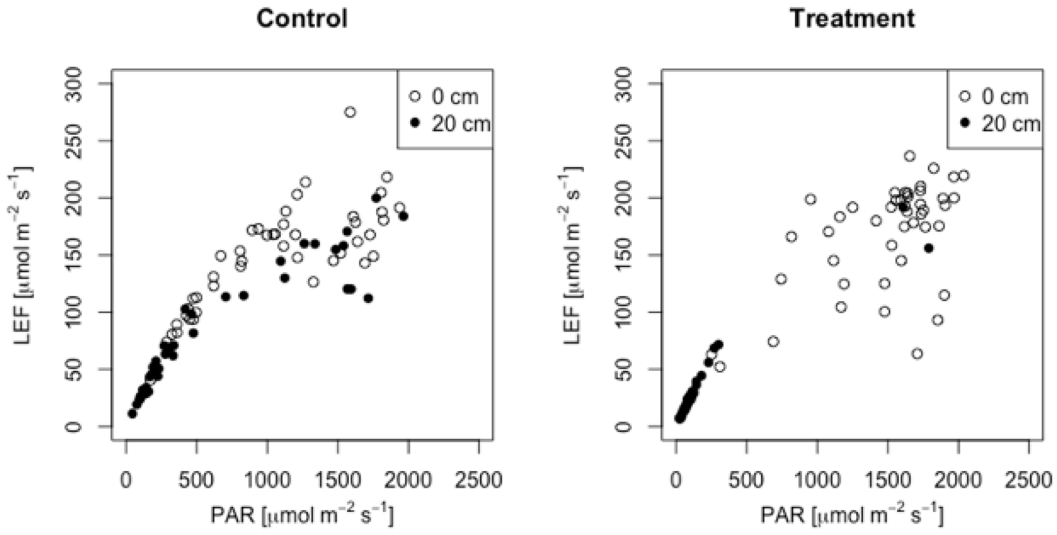

(b) Φ_{II} vs PAR

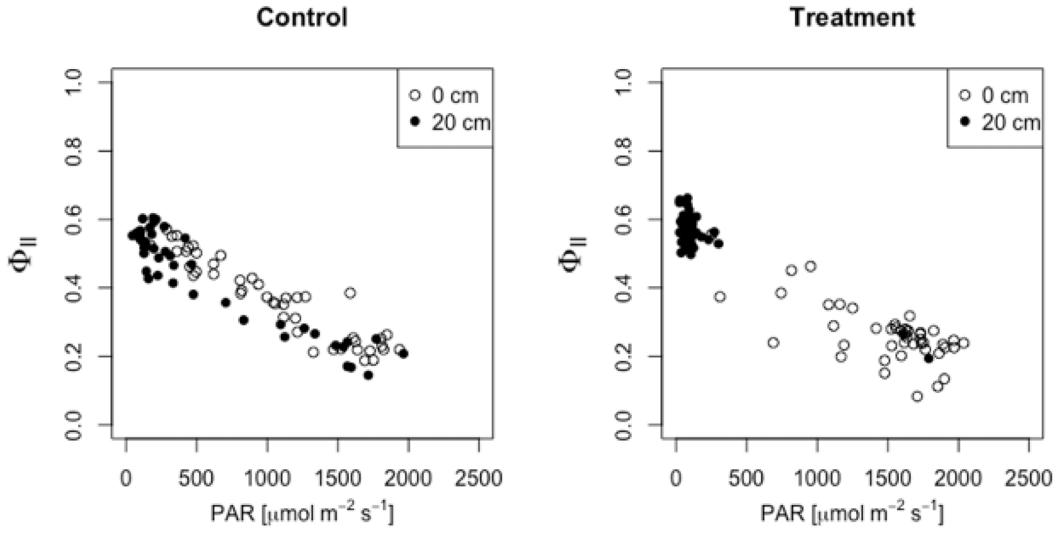

Fig. 4-7

Relation of photosynthetic active radiation (PAR) to Linear electron flow (LEF), photosystem II quantum yield (Φ_{II}), photochemical quenching (q_P), and quantum yield of open photosystem II (Fv'/Fm') at various depths in the kudzu canopy in the control and treatment plots.

(c) q_P vs PAR

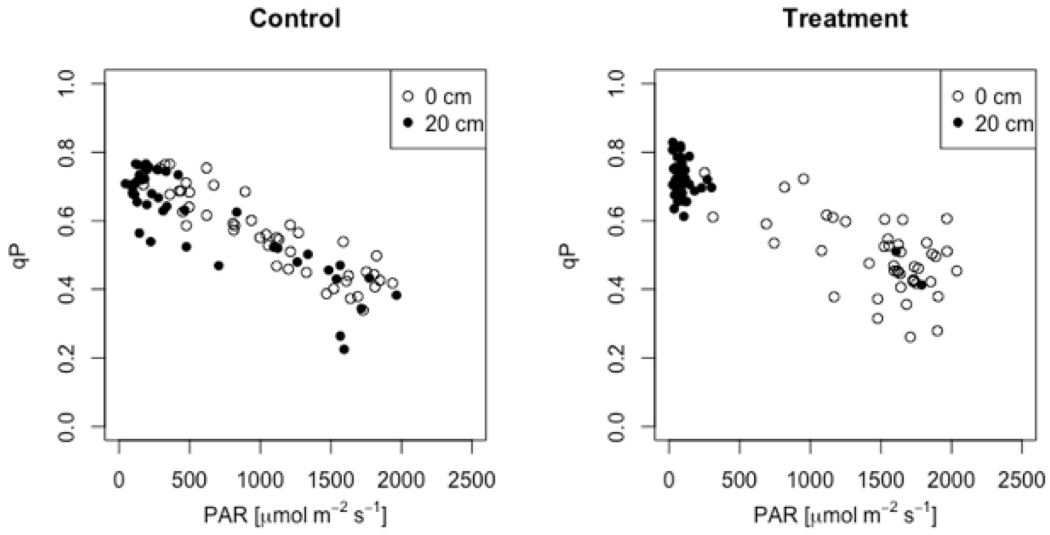

(d) Fv'/Fm' vs PAR

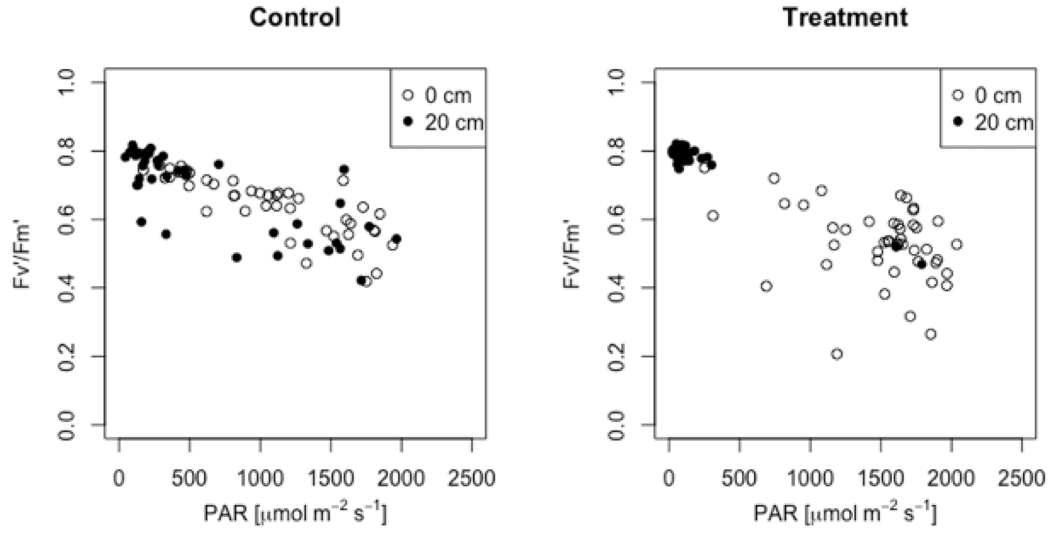

Fig. 4-7 (continued)

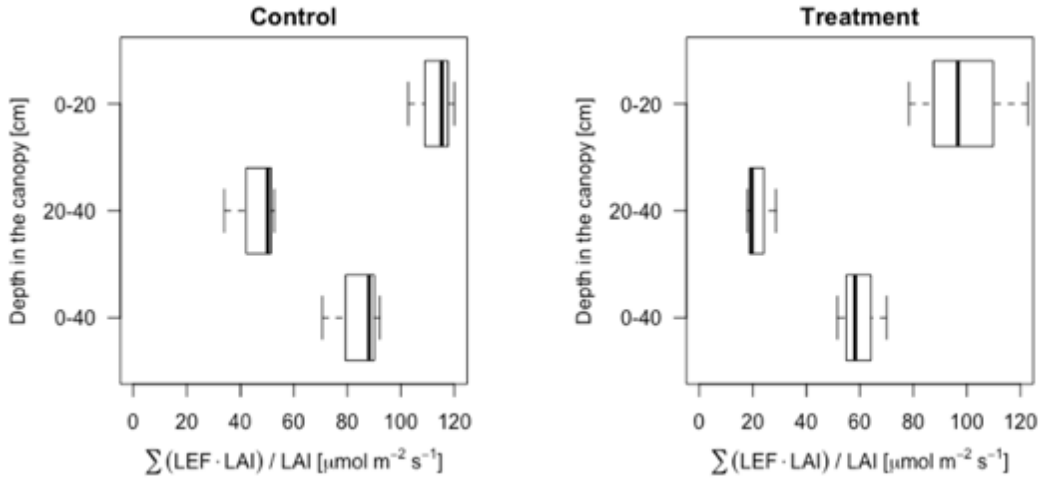

Fig. 4-8

Integrated linear electron flow (LEF) with respect to leaf area index (LAI), an indicator of photosynthetic productivity, at various layers in the kudzu canopy in the control and treatment plot.

The line in the box indicates the median, the box indicates the first and third quantiles, and the whiskers indicate the highest/lowest value that is within 1.5 times the interquartile range from the box. The outliers indicate the data beyond the end of the whiskers.

(a) NPQt vs PAR

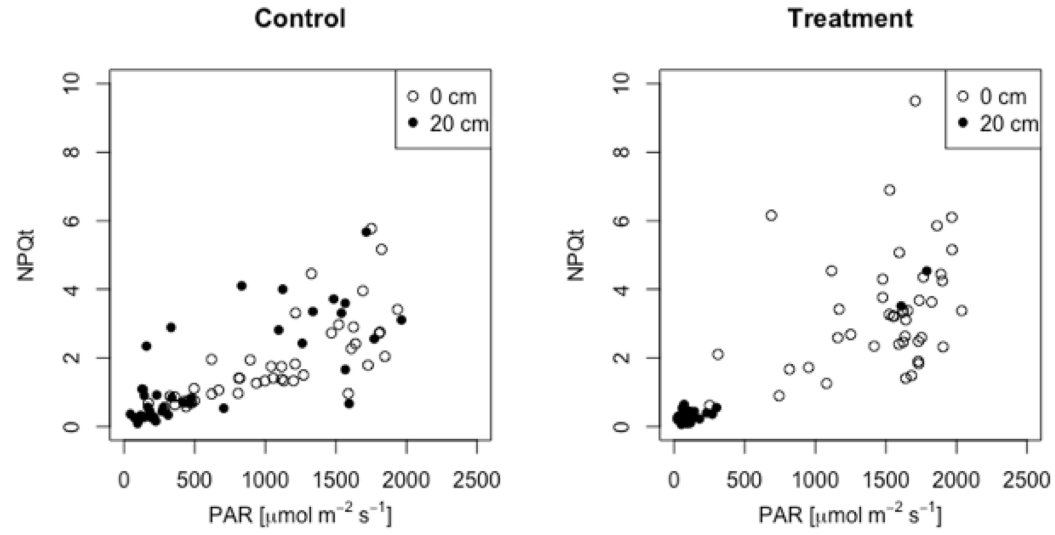

(b) ECSt vs PAR

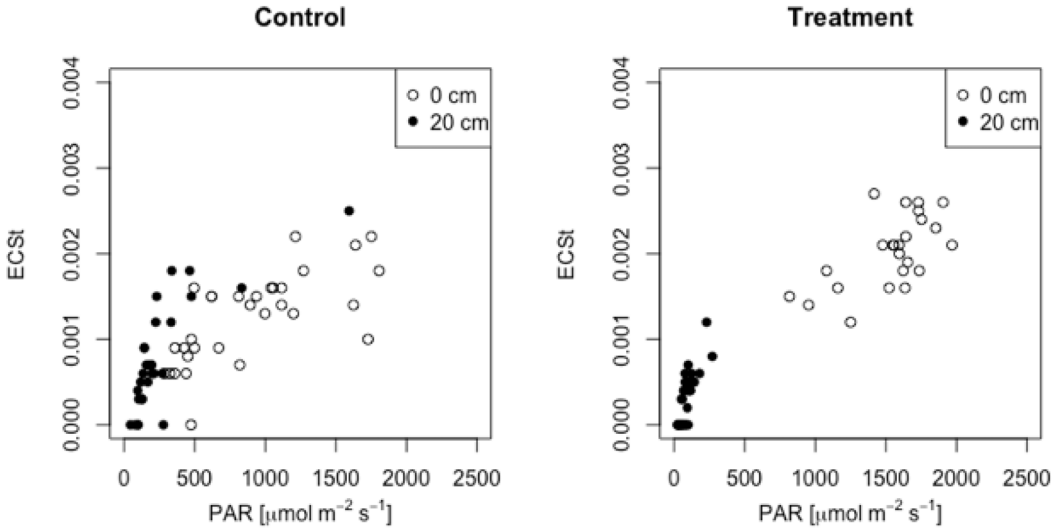

Fig. 4-9

Relation of photosynthetic active radiation (PAR) to NPQt, ECSt at various depths in the kudzu canopy of the control and treatment plots.

(a) NPQt vs LEF

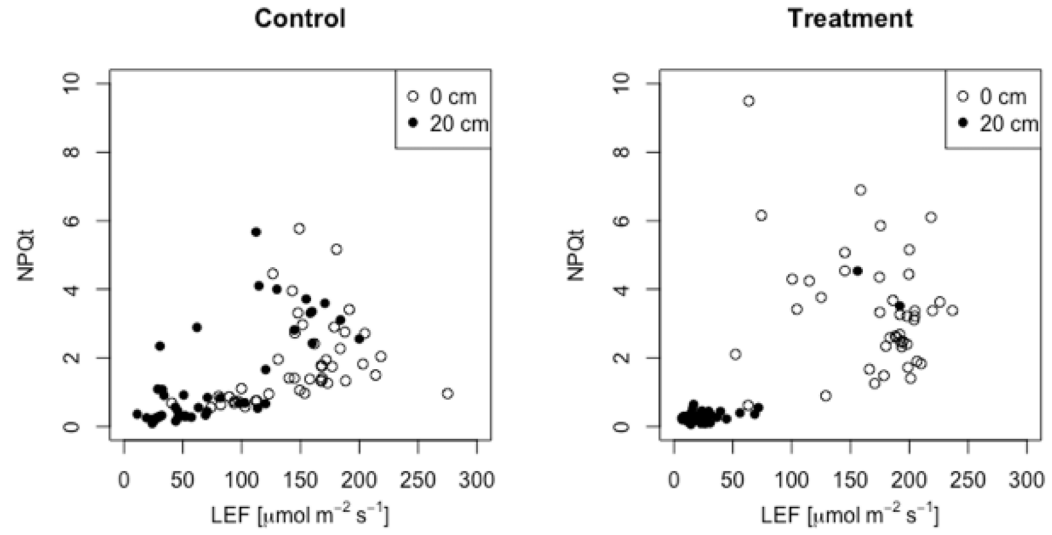

(b) ECSt vs LEF

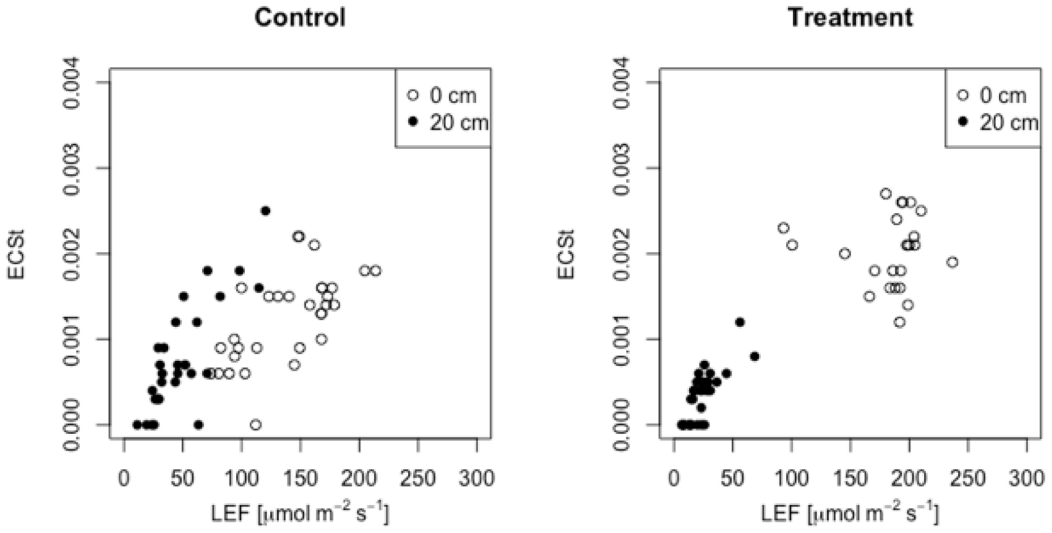

Fig. 4-10

Relation of linear electron flow (LEF) to NPQt, ECSt, and νH^+ at various depths in the kudzu canopy of the control and treatment plots.

(c) vH^+ vs LEF

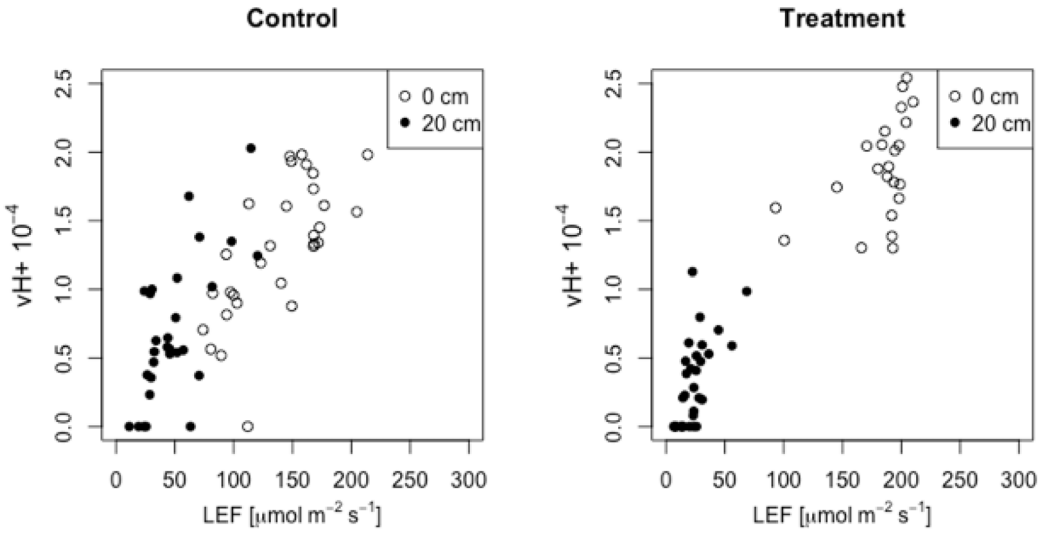

Fig. 4-10 (continued)

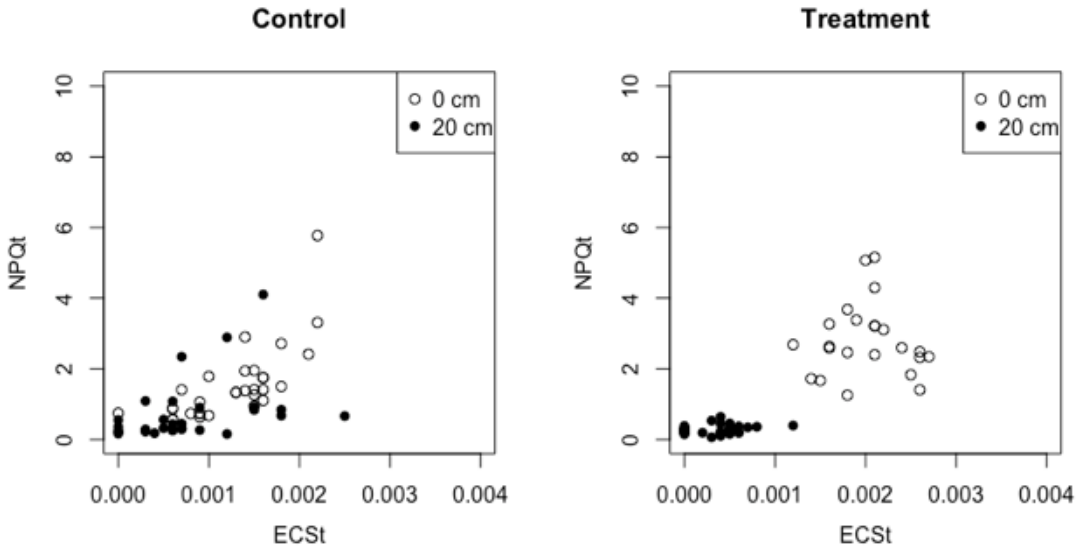

Fig. 4-11

Relation of ECSt to NPQt at various depths in the kudzu canopy of the control and treatment plot.

Chapter 5

General discussion

Ecological traits and optimal management of kudzu

The novel methods of sensing and modeling have contributed to revealing some important traits on photosynthetic function and spatial dynamics of kudzu. The translocation of leaves from the center to the margin of a community (Chapter 2) seems to contribute to the photosynthetic efficiency of the kudzu canopy. Generally, a leaf of an erect herbaceous plant is expanded on the top of the plant, and thereafter, the plant gets covered in new leaves. The gradual change in light intensity is highly correlated to the vertical gradient of leaf nitrogen content in a canopy (DeJong *et al*. 1989). A leaf on a vine is exposed to intense radiation for a relatively longer period by creeping on the ground horizontally and climbing on other objects and experiences various light conditions depending on the growth of the vine. A tree extends its branches and leaves selectively in the direction in which the density of trees is lower to avoid mutual shading (Jones and Harper 1987a, Jones and Harper 1987b). Therefore, plasticity in the canopy structure of vines is much higher. Vine can change leaf nitrogen distribution based on light (Hikosaka et al. 1994, Hikosaka 1996). In addition, some vine legumes including kudzu can improve light penetration by diurnal leaf movement. This behavior is effective, especially when vines grow vertically on some object and its leaves overlap with each other. Leaf orientation also affects leaf age and nitrogen allocation in a community. To examine the effect of the movement, photosynthetic efficiency in the center and margin of a community should be measured and compared in the process of growth.

Such a variable behavior of vines forces the leaves to be exposed to intense and fluctuating radiation. According to field fluorometry (Chapter 4), kudzu adopts multiple mechanical and physiological mechanisms to avoid photoinhibition. The uppermost leaves of a canopy can avoid intense radiation by leaf orientation. The lower leaves are exposed to sunflecks, but they achieve higher photosynthetic productivity by quenching excess energy. To further investigate kudzu's strategy against various light conditions, its mechanical, anatomical, and physiological responses must be analyzed dynamically. The tissue distribution in kudzu is typical of mesophytic species (Pereira-Netto *et al*. 1999), but anatomical responses to light conditions should be considered as part of the photosynthetic acclimation mechanism. The increase in the area of chloroplast surface

facing the intercellular space per unit leaf area contributes to the light-saturated photosynthetic rate of some woody species after gap formation but two climbing species (*Schizophragma hydrangeoides* Sieb. et Zucc. and *Hydrangea petiolaris* Sieb. et Zucc.) did not change their anatomical traits significantly in response to light intensity (Oguchi *et al.* 2006). This fact implies that vine species adopt different strategies for light conditions in their canopy.

The growth towards the margin also plays an important role in community expansion. Higher shoot density makes the growth rate and dry matter of roots and stems smaller (Tsugawa *et al*. 1989) and therefore, expansion of community is important to maximize production. Shoots emerge from rooted nodes of overwintering stems, even if the aboveground organs have been removed. Nodes on the ground root mainly in June, July, and September (Obayashi 1979) and carbohydrate is transported to storage organs after September (Rashid *et al.* 2017). According to the findings of this study (Chapter 2), kudzu expands its community through the expansion of stems and leaves to the margin during midsummer. Kudzu seems to expand the area where shoots are to emerge in the next season by rooting and transporting photosynthetic products to storage organs at the margin of the community after September.

The spatial aggregation of leaves decreases through their translocation towards the margin of the community. In addition, the number of rooted nodes of kudzu decrease and their spatial distribution becomes more uniform as they become older (Tsugawa and Kayama 1974, Tsugawa and Kayama 1975, Tsugawa and Kayama 1978). These evidences suggest that the spatial aggregation of kudzu is mitigated through both, the translocation of leaves in the growing season and degradation of storage organs. Competitively superior plant species have lower biomass in aggregated distribution, probably because within a community, individuals interfere more often with conspecies (Stoll and Prati 2001, Monzeglio and Stoll 2005). Kudzu might mitigate aggregation within its community to decrease the frequency of intraspecific competition.

The regeneration of leaves costs a huge amount of photosynthetic product. When a new stem encounters inappropriate conditions, the cost for expansion cannot be collected by photosynthesis and kudzu lose resources for propagation. Partly, leaf orientation can contribute to avoiding intense radiation and drought. In addition, expansion toward the margin also increases the frequency of interspecific competition. Kudzu can climb other plants and cover them with leaves, but vertical climbing prevents horizontal extension

and rooting on the ground. Kudzu can also propagate by producing seeds. The seeds have deep dormancy, which is broken by fire and scarring (Fukuda 2014). Therefore, kudzu can emerge from seeds after drastic disturbances, even if it is not competitive enough with other plants.

These evidences indicate that the prevention of rooting and accumulation of carbohydrates into storage organs by removing higher-order branches, especially in the margin of community in midsummer, is effective for the containment of the kudzu community. Undoubtedly, it is best to completely remove crown roots and overwintering stems; however, it unrealistic in terms of cost. The complete suppression of the emergence of shoots and growth of branches from residual stems and roots after mowing in summer is impossible. Nevertheless, the removal of the aboveground organs repeatedly should be effective in suppressing the emergence of stems after the next season by reducing carbohydrate storage potential. However, mowing may also promote the rooting of nodes. Arase *et al.* (1999) found that there exists a trade-off relationship between emigration by stem and settlement by penetration into the soil in yabumame (*Amphicarpaea edgeworthii* Benth.). In addition, mowing in midsummer is tough and dangerous in Japan. It is also important to prevent invasion and rooting into virgin territories by laying sheets in front of the community. The application of herbicide to crowns (Tanaka *et al*. 2008, Tanaka *et al*. 2009) and removal of storage organs (Nishino *et al*. 2019) needs to be examined simultaneously. The effect of spatial and temporal variations in disturbances on community dynamics should be evaluated for further examination of optimal management. It can be described in the hierarchical model and should be examined by long-term monitoring of kudzu community in the field.

Improvement of sensing and modeling for weed science

In this thesis, I have demonstrated the usefulness of novel sensing technologies in weed science. A particular species of weed can be extracted from UAV imagery by machine learning. The serial sensing of the kudzu community revealed the spatial translocation of the leaves and the temporal variation of the spatial dynamics. A spatial dynamic model based on serial sensing data should be valuable to optimize resource allocation to contain the community. In addition, field fluorometry is useful to evaluate the photosynthetic efficiency of the wild weed community in real time. To utilize sensing data as features of weed community and to extract information for practical management,

sensing techniques should be combined with flexible model and its comprehension based on coherent insight into weed ecology.

The classification of occupancy was based on the average brightness in each 50 × 50 cm grid. This indicates that kudzu can be detected on images with lower resolution. Vegetation dynamics might be monitor in a wider area based on satellite imagery in the future. Additionally, such nondestructive and labor-saving measurements of vegetation enable us to evaluate spatial distribution dynamically rather than statically. UAV has an advantage in the monitoring and simulation of weed community dynamics for image obtainment. UAV image processing should be examined, especially in the early and late stages of growth. Both, the model and parameters should be evaluated and selected to improve the accuracy of weed detection. In the case of species showing aggregated distribution, such as kudzu, the distribution should have some spatial autocorrelation. For example, Poggi *et al*. (2005) used the tree-structured Markov random field (MRF) model for remote sensing image segmentation. The parameters on the observation model should consider spatial autocorrelation. More parameters for classification can be extracted from aerial imagery. The shape of weeds from the pattern of pixels may be useful for distinguishing species that have resembling leaf colors. The height based on the digital surface model (DSM) can also serve as valuable information. When hyperspectral reflectance is available, it will be useful to classify species and to estimate abundance precisely (Haboudane *et al*. 2004, Suzuki *et al.* 2010). However, the algorithm may be too complicated for humans to decipher in the case of many variables. In such cases, it would be beneficial to reduce the features by principal component analysis (PCA).

As demonstrated, the combination of UAV imagery and HMM is appropriate to estimate occupancy dynamics. Intervals of observation and spatial resolution of imagery can be adjusted easily by UAV according to the rate of emergence, growth, and expansion of target species. When intervals are not constant for weather or other conditions, occupancy dynamics should be described in the Markov process with missing values or the Gaussian process (Roberts *et al*. 2013). Plant community dynamics may include many latent states. It is necessary to incorporate the transition of storage organs, especially, for long-term simulation of weed population dynamics. Hughes *et al.* (2014) described the process of above- and below-ground organs of kudzu in parallel. However, they are invisible in aerial imagery and the survey might be destructive and labor-consuming. Buried seeds and storage organs of perennial plants are hardly reflected in the spectral

reflectance. HMM is essential to model and simulate weed community dynamics based on sensing data because it can deal with 'hidden' states. Dry weight, leaf area, height, and the number of individuals can also be incorporated into the hierarchical model instead of binomial presence/absence data. State space model (SSM) deal with states taking on continuous values, while HMM deals with states taking on only finite discrete values. Each parameter in an ecological process often includes some spatial factors that reflect the morphological features and propagation strategy of each weed species or population. How should it be incorporated into the model? When the process of growth is observed, the construction can be evaluated by incorporating the process into the dynamic model. In contrast, in case the spatial construction has already been established, it should be incorporated into the model statically. Hierarchical models enable incorporating spatial construction, such as spatial autocorrelation, flexibly. In addition, habitat type might affect the growth of organs (Waite 1994). Incorporating spatial heterogeneity in habitat type and environmental factors should be effective to model the long-term dynamics of a weed community.

Techniques for real-time monitoring of photosynthesis in the field need to be developed further. Solar-induced fluorescence (SIF) can measure chlorophyll fluorescence remotely even from satellites (Frankenberg *et al*. 2011); however, the spatial resolution is not sufficient for weed canopy. However, some photosynthetic parameters can be evaluated using spectrometry by remote sensing. SAVI has been proved to be correlated to canopy evaporation (Choi and Inoue 2004). Cl_{green} (Gitelson *et al*. 2003) can be utilized for the estimation of gross production capacity (Thanyapraneedkul *et al*. 2012). Photochemical reflectance index (PRI) (Gamon *et al.* 1992), based on the difference in the absorbance of xanthophyll pigment by epoxidation state, can be calculated from narrow-band reflectance. It has been proved to correlate with light use efficiency (e.g., Nichol *et al*. 2000). Real-time monitoring of physiological activity should be developed and sophisticated practically, to evaluate plants' plasticity to environment condition and seasonal change.

Further extension of sensing and modeling in weed science

The models of spatial distribution can be extended to multiple species. Many indicators have been proposed to evaluate spatial heterogeneity based on the composition of species, for example, power law index (Shiyomi *et al*. 2001), Shannon-Wiener index

(Shannon 1948), Bray-Curtis dissimilarity (Bray and Curtis 1957). The application of remote sensing data to these indicators can contribute to understanding the spatial distribution of species.

Interaction with other species affects the rate of colonization and growth. Interspecific competition can be incorporated into the dynamic model. Lotka-Volterra model should be appropriate to describe competition with each other when multiple species are considered to exist together in a grid. When the process of translocation is considered, the probability of colonization from the adjacent grids can depend on the other species occupying the grid or the abundance of species. In addition, the effect of disturbance on each species' distribution can be simulated by this model. Spatial and temporal variation of disturbance affects the dynamics of species composition (Ohsawa *et al*. 2002). Incorporating disturbance into the model can enable to simulate the influence of management on the process of succession. When processes of growth and colonization are incorporated appropriately, the simulation of spatial dynamics in the future, based on state space models can be valuable in developing weed management strategies. Flesh weight of weeds is highly correlated to mowing cost (Nishimuta and Yanase 2016) and estimating the growth of weed based on remote sensing will contribute to optimal allocation of limited efforts. Time-series spatial sensing data and hierarchical model should be combined into a system for estimating the occupancy and growth of weeds. As a precedent in grassland management, the National Agriculture Research Organization (NARO) of Japan has developed a grassland management support system (Nishimura and Ide 2017, Kitagawa 2017). This system manages spatial data of grassland on GIS and is useful in visualizing and sharing information. A similar system that integrates sensing data would be valuable for the zoning of vegetation and prioritization of weed management.

The combination of sensing data on architectural structure and physiological function leads to a comprehensive understanding of plant growth and competition. The architectural structure of plants affects intraspecific and interspecific competition through light interception. 3D architecture can be scanned by novel sensing techniques. UAV can obtain a DSM of a canopy by multidirectional sensing. Light detection and ranging (LiDAR) can measure vertical structure inside a canopy. The L-system (Prusinkiewicz 2004) and volumetric pixel (voxel) model (Hosoi and Omasa 2006) are suitable to describe and simulate the 3D structures of individual plants and their canopies based on

measurement (Lewis 1999, Kim *et al*. 2016). Obtaining time-series data of 3D architecture is valuable for the evaluation of 3D spatial occupancy dynamics. Some models in which sensing data can be incorporated have been proposed for the evaluation of plant growth and interaction. Ecophysiological models, describing growth hierarchically based on canopy structure and dry matter production, have been developed for crop-weed competition and yield loss (Bastiaans *et al*. 2000). The functional-structural plant model (FSPM), which includes light environment and photosynthesis, has been improved in crop management for competition to weeds (Vos et al. 2010, Evers and Bastiaans 2016). Sensing technology and flexible modeling enables us to describe the development of the 3D structure of plants as governed by physiological processes over time.

Novel sensing technologies change data in quality and quantity. Objective information should be extracted from data with higher dimension and resolution, efficiently and reproducibly. For weed management, we should simulate the dynamics with flexible model and its comprehension. The compilation of knowledge on ecological traits and frameworks of data processing will be valuable for hacking weed community dynamics.

References

Alexandridis, T. K., Tamouridou, A. A., Pantazi, X. E., Lagopodi, A. L., Kashefi, J., Ovakoglou, G. V., ... & Moshou, D. (2017). Novelty detection classifiers in weed mapping: *Silybum marianum* detection on UAV multispectral images. *Sensors 17*, 2007.

Anselin, L. (1995). Local indicators of spatial association – LISA. *Geographical Analysis 27*, 93–115.

Araki, M. (2014). Introduction of machine learning with free software. Morikita Press, Tokyo, pp. 115-127. [in Japanese]

Arase *et al.* (1999). Growth and seed yield of *Amphicarpaea edgeworthii* Benth. in a field cropping. *Japanese Journal of Crop Science 68*, 83-90.

Asada, M., Osada, Y., Fukasawa, K. & Ochiai, K. (2014). Bayesian estimation of reeves' muntjac (*Muntiacus reevesi*) populations using state-space models. *Mammalian Science 54*, 53-72.

Auld, B. A. & Johnson, S. B. (2014). Invasive alien plant management. *CAB reviews 9*, 37.

Aurambout, J. P. & Endress, A. G. (2018). A model to simulate the spread and management cost of kudzu (*Pueraria montana* var. *lobata*) at landscape scale. *Ecological Informatics 43*, 146-156.

Bakhshipour, A. & Jafari, A. (2018). Evaluation of support vector machine and artificial neural networks in weed detection using shape features. *Computers and Electronics in Agriculture 145*, 153-160.

Bastiaans, L., Kropff, M. J., Goudriaan, J. & van Laara, H. H. (2000). Design of weed management systems with a reduced reliance on herbicides poses new challenges and prerequisites for modeling crop-weed interactions. *Field Crops Research 67*, 161-179.

Bivand, R. S. & Wong, D. W. S. (2018). Comparing implementations of global and local indicators of spatial association. *TEST 27*, 716–748

Bonsi, C., Rhoden, E., Woldeghebriel, A., Mount, P., Solaiman, S., Noble, R., Paris, G., McMahon, C., Pearson, H. & Cash, B. (1992). Kudzu-goat interactions — A pilot study. In: Solaiman, S. G. & Hill, W. A. (Eds.) *Using goats to manage forest vegetation,*

a regional inquiry. Tuskegee, AL: Tuskegee University Agricultural Experiment Station. pp. 84-88.

Boyne, R., Osunkoya, O. O. & Scharaschkin, T. (2013). Variation in leaf structure of the invasive Madeira vine (*Anredera cordifolia*, Basellaceae) at different light levels. *Australian Journal of Botany 61*, 412–417.

Bray, J. R. & Curtis, J. T. (1957). An ordination of upland forest communities of southern Wisconsin. *Ecological Monographs 27*, 325-349.

Chabot, D., Dillon, C., Shemrock, A., Weissflog, N. and Sager, E. P. S. (2018). An Object-Based Image Analysis Workflow for Monitoring Shallow-Water Aquatic Vegetation in Multispectral Drone Imagery. *International Journal of Geo-Information 7*, 294.

Choi, E. & Inoue, Y. (2004). Relationship of transpiration and evapotranspiration to solar radiation and spectral reflectance in soybean canopies — A simple method for remote sensing of canopy transpiration —. *Journal of Agricultural Meteorology 60*, 43-53.

Cruz, J. A., Sacksteder, C. A., Kanazawa, A. & Kramer, D. M. (2001). Contribution of electric field (ΔΨ) to steady-state transthylakiod proton motive force (*pmf*) in vitro and in vivo. Control of *pmf* parsing into ΔΨ and ΔpH by ionic strength. *Biochemistry 40*, 1226-1237.

Dejong, T. M., Day, K. R. & Johnson, R. S. (1989). Seasonal relationships between leaf nitrogen content (photosynthetic capacity) and leaf canopy light exposure in peach (*Prunus persica*). *Trees 3*, 89-95.

Evers, J. B. & Bastiaans, L. (2016). Quantifying the effect of crop spatial arrangement on weed suppression using functional-structural plant modelling. *Journal of Plant Research 129*, 339-351.

Ferguson, P. F. B., Conroy, M. J. & Hepinstall-Cymerman, J. (2015). Occupancy model for data with false positive and false negative errors and heterogeneity across sites and surveys. *Methods in Ecology and Evolution 6*, 1395-1406.

Fernández-Calleja, M., Monteagudo, A., Casas, A.M., Boutin, C., Pin, P.A., Morales, F. & Igartua, E. (2020). Rapid on-site phenotyping via field fluorimeter detects

differences in photosynthetic performance in a hybrid - parent barley germplasm set. *Sensors 20*, 1486.

Field, C. (1983). Allocating leaf nitrogen for the maximization of carbon gain: Leaf age as a control on the allocation program. *Oecologia*. *56*, 341-347.

Forseth, I. N. & Teramura, A. H. (1986). Kudzu leaf energy budget and calculated transpiration: the influence of leaflet orientation. *Ecology 67*, 564-571.

Forseth, J. I. N. & Innis, A. F. (2004). Kudzu (*Pueraria montana*): History, physiology, and ecology combine to make a major ecosystem threat. *Critical Reviews in Plant Sciences 23*, 401-413.

Frankenberg, C., Butz, A. & Toon, G. C. (2011), Disentangling chlorophyll fluorescence from atmospheric scattering effects in O_2 A-band spectra of reflected sun-light. *Geophysical Research Letters 38,* L03801.

Frye, M. J., Hough-Goldstein, J., & Sun, J. H. (2007). Biology and preliminary host range assessment of two potential kudzu biological control agents. *Envionmental Entomology 36*, 1430-1440.

Frye, M. J., Hough-Goldstein, J. & Kidd, K. A. (2012). Response of kudzu (*Pueraria montana* var. *lobata*) to different types and levels of simulated insect herbivory damage. *Biological Control 61*, 71-77.

Frye, M. J. & Hough-Goldstein, J. (2013). Plant architectute and growth response of kudzu (Fabales: Fabaceae) to simulated insect herbivory. *Environmental Entomology 42*, 936-941.

Fukuda, E. (2014). Influences of clear-cutting, burning and sheep grazing on the dynamics of buried seeds of kudzu (*Pueraria lobata* (Willd.) Ohwi) in abandoned land. *Japanese Journal of Grassland Science 60*, 1-9.

Gamon, J. A., Penuelas, J. & Field, C. B. (1992). A narrow-waveband spectral index that tracks diurnal changes in photosynthetic efficiency. *Remote Sensing of Environment 41*, 35-44.

Gelman, A. & Rubin, D. B. (1992). Inference from iterative simulation using multiple sequences. *Statistical Science 7*, 457-472.

Geographical Survey Institute. (2019). Conversion into plane rectangular coordinate system. https://vldb.gsi.go.jp/sokuchi/surveycalc/surveycalc/bl2xyf.html (Access confirmed on 2021. 3. 1.)

Getis, A. & Ord, J. K. (1992). The analysis of spatial association by use of distance statistics. *Geographical Analysis 24*, 189-205.

Gitelson, A. A., Merzlyak, M. N. & Lichtenthaler, H. K. (1996). Detection of red edge position and chlorophyll content by reflectance measurements near 700nm. *Journal of Plant Physiology 148*, 501-508.

Gitelson, A. A. & Merzlyak, M. N. (1997). Remote estimation of chlorophyll content in higher plant leaves. *International Journal of Remote Sensing 18*, 2691-2697.

Gitelson, A. A., Gritz, Y. & Merzlyak, M. N. (2003). Relationships between leaf chlorophyll content and spectral reflectance and algorithms for non-destructive chlorophyll assessment in higher plant leaves. *Journal of Plant Physiology 160*, 271-282.

Haboudane, D., Miller, J. R., Pattey, E., Zarco-Tejada, P. J. & Strachan, I. B. (2004). Hyperspectral vegetation indices and novel algorithms for predicting green LAI of crop canopies: Modeling and validation in the context of precision agriculture. *Remote Sensing of Environment 90*, 337–352.

Hikosaka, K., Terashima, I. & Katoh, S. (1994). Effects of leaf age, nitrogen nutrition and photon flux density on the distribution of nitrogen among leaves of a vine (*Ipomoea tricolor* Cav.) grown horizontally to avoid mutual shading of leaves. *Oecologia 97*, 451-457.

Hikosaka, K. (1996). Effects of leaf age, nitrogen nutrition and photon flux density on the organization of the photosynthetic apparatus in leaves of a vine (*Ipomoea tricolor* Cav.) grown horizontally to avoid mutual shading of leaves. *Planta 198*, 144-150.

Hikosaka, K. (2003).A model of dynamics of leaves and nitrogen in a plant canopy: an integration of canopy photosynthesis, leaf life span, and nitrogen use efficiency. *The American Naturalist 162*,149-164.

Hoffberg, S. L., Mauricio, R. & Hall, R. J. (2018). Control or re-treat? Model-based guidelines for managing established plant invasions. *Biological Invasions 20*, 1387-1402.

Horler, D. N., Dockray, M. & Barber, J. (1983). The red edge of plant leaf reflectance. *International Journal of Remote Sensing 4*, 273-288.

Hosoi, F. & Omasa, K. (2006). Voxel-based 3-D modeling of individual trees for estimating leaf area density using high-resolution portable scanning lidar. *IEEE*

Transactions on Geoscience and Remote Sensing 44, 3610-3618.

Huete, A. R. 1988. A soil vegetation adjusted index (SAVI). *Remote Sensing of Environment 25*, 295-309.

Hughes, M. J., Johnson, E. G. & Armsworth, P. R. (2014). Optimal spatial management of an invasive plant using a model with above- and below-ground components. *Biological Invasions 16*, 1009-1020.

Inoue, Y., Miah, G., Sakaiya, E., Nakano, K. & Kawamura, K. (2008). NDSI map and IPLS using hyperspectral data for assessment of plant and ecosystem variables: with a case study on remote sensing of grain protein content, chlorophyll content and biomass in rice. *Journal of The Remote Sensing Society of Japan 28*, 317-330.

Ishida, A., Toma, T. & Marjenah (1999). Leaf gas exchange and chlorophyll fluorescence in relation to leaf angle, azimuth, and canopy position in the tropical pioneer tree, *Macaranga conifera*. *Tree Physiology 19*, 117-124.

Isoda, A., Yoshimura, T., Ishikawa, T., Nojima, H. & Takasaki, Y. (1993a). Effects of leaf movement on radiation interception in field grown leguminous crops. I. Peanut (*Arachis hypogaea* L.). *Japanese Journal of Crop Science 62*, 300-305.

Isoda, A., Yoshimura, T., Ishikawa, T., Wang, P., Nojima, H. & Takasaki, Y. (1993b). Effects of leaf movement on radiation interception in field grown leguminous crops. II. Soybean (*Glycine max* Merr.). *Japanese Journal of Crop Science 62*, 306-312.

Isoda, A., Misa, A. L., Nojima, H. & Takasaki, Y. (1996). Effects of leaf movement on radiation interception in field grown leguminous crops. IV. Relation to leaf temperature and transpiration among peanut cultivars. *Japanese Journal of Crop Science 65*, 700-706.

Iwasa, Y. & Teramoto, E. (1977). A mathematical model for the formation of a distributional pattern and an index of aggregation. *Japanese Journal of Ecology 27*, 117-124.

Jones, M. & Harper, J. L. (1987a). The influence of neighbours on the growth of trees I. The demography of buds in *Betula pendula*. *Proceedings of the Royal Society London 232*, 1-18.

Jones, M. & Harper, J. L. (1987b). The influence of neighbours on the growth of trees II. The fate of buds on long and short shoots in *Betula pendula*. *Proceedings of the Royal*

Society London 232, 19-33.

Kameyama, A. (1978). Kudzu community in vegetation succession on the slope of expressway. *Journal of Japanese Revegetational Technology Society 5*, 36-42. [in Japanese]

Karatzoglou, A., Smola, A., Hornik, K. & Zeileis, A. (2004). kernlab - An S4 Package for Kernel Methods in R. *Journal of Statistical Software 11(9)*, 1–20.

Katul, G. G., Porporato, A., Nathan, R., Siqueira, M., Soons, M. B., Poggi, D., ... & Levin, S. A. (2005). Mechanistic analytical models for long-distance seed dispersal by wind. *The American Naturalist 166*, 368-381.

Kawamoto, A. (2018). A story of kudzu starch: the past, present and future of Yoshino-honkudzu crafts. *Weeds and Vegetation management 10 (Special Issue)*, 15-21.

Kawamura, K. & Akiyama, T. (2012). Remote sensing for precision grassland management. *Journal of The Remote Sensing Society of Japan 32*, 232-244.

Kawashima, R. (1969). Studies on the leaf orientation-adjusting movement in soybean plants I. The leaf orientation-adjusting movement and light intensity on leaf surface. *Japanese Journal of Crop Science 38*, 718-729.

Kellner, K. (2017). jagsUI: a wrapper around 'rjags' to streamline 'JAGS' analyses. R package version 1.4.4. https://cran.r-project.org/web/packages/jagsUI/index.html (Access confirmed on 2021. 3. 1.)

Kin, M. (2017). Data science by R (Second edition). Morikita Press, Tokyo, pp. 206–215. [in Japanese]

Kim, E., Lee, W. K., Yoon, M., Lee, J. Y., Son, Y., & Salim, K. A. (2016). Estimation of voxel-based above-ground biomass using airborne LiDAR data in an intact tropical rain forest, Brunei. *Forests 7*, 259.

Kitagawa, M. (2017). Efficient grassland management method using the grassland management support system. *Journal of Japanese Grassland Science* 62, 212-215.

Komuro, T. & Koike, F. (2005). Colonization by woody plants in fragmented habitats of a suburban landscape. *Ecologocal Applications 15*, 662-673.

Kramer D. M., Sacksteder, C. A. & Cruz, J. A. (1999). How acidic is the lumen? *Photosynthesis Research 60*, 151-163.

Kosaki, T. & Ito, K. (2018). A story of kudzu fiber textiles: the past, present and future of Kakegawa crafts. *Weeds and Vegetation management 10 (Special Issue)*, 22-27.

Kuhlgert, S., Austic, G., Zegarac, R., Osei-Bonsu, I., Hoh, D., Chilvers, M. I., ... & Kramer, D. M. (2016). MultispeQ Beta: a tool for large-scale plant phenotyping connected to the open PhotosynQ network. *Royal Society Open Science 3*, 160592.

Lang, A. R. G. (1973). Leaf orientation of a cotton plant. *Agricultural Meteorology 11*, 37-51.

Lamiter, A. M., Wu, S., Gelfand, A. E. & Silander Jr., J. A. (2006). Building statistical models to analyze species distributions. *Ecological Applications 16*, 33-50.

Lewis, P. (1999). Three-dimensional plant modelling for remote sensing simulation studies using the Botanical Plant Modelling System. *Agronomie 19*, 185-210.

Liu, H. K., Gyokusen, K., & Saito, A. (1997a). Studies on leaf orientation movements in kudzu (*Pueraria lobata*) (I): Diurnal changes of leaflet azimuth and leaf temperature. *Bulletin of the Kyushu University Forest 76*, 11-24.

Liu, H. K., Gyokusen, K., & Saito, A. (1997b). Studies on leaf orientation movements in kudzu (*Pueraria lobata*) (II): Effects of leaf orientation movements on photosynthetic rate. *Bulletin of the Kyushu University Forest 77*, 1-12.

Lopez-Granados, F., Torres-Sanchez, J., De Castro, A.-I., Serrano-Perez, A., Mesas-Carrascosa, F.-J. & Pena, J.-M. (2016). Object-based early monitoring of a grass weed in a grass crop using high resolution UAV imagery. *Agronomy for Sustainable Development 36*, 67.

Louargant, M., Villette, S., Jones, G., Vigneau, N., Paoli, J. N. & Gee, C. (2017). Weed detection by UAV: simulation of the impact of spectral mixing in multispectral images. Precision Agriculture 18, 932-951.

Louvrier, J., Chambert, T. Marboutin, E. & Gimenez, O. (2018). Accounting for misclassification and heterogeneity in occupancy studies using hidden Markov models. *Ecological modelling 387*, 61-69.

McClintock, B. T., Langrock, R., Gimenez, O., Cam, E., Borchers, D. L., Glennie, R. & Patterson, T. A. (2020). Uncovering ecological state dynamics with hidden Markov models. *Ecological Letters 23*, 1878-1903.

Miller, J. H. & Edwards, B. (1983). Kudzu: where did it come from? And how can we stop it? *Southern Journal of Applied Forestry 7*, 165-169.

Miller, D. A. W., Weir, L. A., McClintock, B. T., Campbell Grant, E. H., Bailey, L. L. & Simons, T. R. (2012). Experimental investigation of false positive errors in auditory species occurrence surveys. *Ecological Applications 22*, 1665–1674.

Monteith, J. L. (1977). Climate and the efficiency of crop production in Britain. *Philosophical Transactions of the Royal Society B* 281, 277-294.

Monzeglio, U. & Stoll, P. (2005). Spatial patterns and species performances in experimental plant communities. *Oecologia 145*, 619-628.

Muranaka, T. & Washitani, I. (2003). The population expansion predicted by a simulation model of an invasive alien species, *Eragrostis curvula*, in a middle reach floodplain. *Japanese Journal of Conservation Ecology 8*, 51-62.

Nathan, R., Klein, E., Rebledo-Arnuncio, J. J. and Revilla, E. (2012). Dispersal kernels: review. Oxford University Press. pp. 189-210.

Nemoto, M. (2001). Method for weed community structure. in Weed Science Society of Japan (eds.) “Method in Weed Science”, Weed Science Society of Japan, Tokyo, pp. 63-75.

Nichol et al. (2000). Remote sensing of photosynthetic-light-use efficiency of boreal forest. Nichol, C. J., Lloyd, J., Shibistova, O., Arneth, A., Röser, C., Knohl, A., Matsubara, S. & Grace, J. (2002). Remote sensing of photosynthetic-light-use efficiency of a Siberian boreal forest. *Tellus B: Chemical and Physical Meteorology 54*, 677-687.

Nishimura, K. & Ide, Y. (2017). Development of “grassland management support system” to rationalize ranch management. *Journal of Japanese Grassland Science* 62, 207-211.

Nishimuta, K. & Yanase, T. (2016). The model using the plant height to determine the timing to mow vegetation on embankment slopes. *Journal of Japanese Society of Revegetation Technology 42*. 98-103.

Nishino, A., Maebara, Y., Hasimoto, K., Uchida, T. and Hayasaka, D. (2019). Search for the eradication techniques on the noxious liana kudzu (*Pueraria lobata* (Willd.) Ohwi) in consideration of cut-slope vegetation recovery. *Journal of Japanese Society Revegetation Technology 44*, 596-605.

Obayashi, K. (1979). Ecology of kudzu from the viewpoint of forest nursery. *Ringyo Gijutu 444*, 231-235. [in Japanese]

Oguchi, R., Hikosaka, K., Hiura, T. & Hirose, T. (2006). Leaf anatomy and light acclimation in woody seedlings after gap formation in a cool-temperate deciduous forest. *Oecologia 149*, 571-582.

Oguma, H., Ide, R. & Isagi, Y. (2016). Automatic detection of the flowers of endangered vegetation by unmanned aerial vehicle observation. *Journal of The Remote Sensing Society of Japan 36*, 72-80.

Okazaki (Tanaka), M., Hanawa, S. & Masaru Ogasawara, M. (2018). Growth of climbing vines and pod production of Kudzu (*Pueraria lobata* (Willd.) Ohwi.). *Journal of the Japanese Society of Revegetation Technology 43*, 620-622.

Osawa, T., Okawa, S., Kurokawa, S. & Ando, S. (2016). Generating an agricultural risk map based on limited ecological information: A case study using *Sicyos angulatus*. *Ambio 45*, 895–903.

Pagel, J. & Schurr, F. M. (2012). Forecasting species ranges by statistical estimation of ecological niches and spatial population dynamics. *Global Ecology and Biogeography 21*, 293-304.

Pereira-Netto, A. B., Gabriele, A. C. & Pinto, H. S. (1999). Aspects of leaf anatomy of kudzu (*Pueraria lobata*, Leguminosae-Faboideae) related to water and energy balance. *Pesquisa Agropecuária Brasileira 34*, 1361-1365.

Plummer, M. (2003). JAGS: A program for analysis of Bayesian graphical models using Gibbs sampling. *Proceedings of the 3rd international workshop on distributed statistical computing 124*, 125.

Poggi, G., Scarpa, G. & Zerubia, J. B. (2005). Supervised segmentation of remote sensing images based on a tree-structured MRF model. *IEEE Transactions on Geoscience and Remote Sensing 43*, 1901–1911.

Prusinkiewicz, P. (2004). Modeling plant growth and development. *Current Opinion in Plant Biology 7*, 79–83.

QGIS.org. (2021). QGIS Geographic Information System. QGIS Association. http://www.qgis.org (Access confirmed on 2021. 3. 1.)

Rashid, Md. H., Uddin, Md. N., Asaeda, T. & Robinson, R. W. (2017). Seasonal variations of carbohydrates in *Pueraria lobata* related to growth and phenology. *Weed Biology and Management 17*, 103-111.

Rasmussen, J., Georgios, N. Nielsen, J., Svesgaard, J., Poulsen, R. N. & Christensen, S. (2016). Are vegetation indices derived from consumer-grade cameras mounted on UAVs sufficiently reliable for assessing experimental plots? *European Journal of Agronomy 74*, 75-92.

R Core Team (2019). R: A language and environment for statistical computing. R Foundation for Statistical Computing, Vienna, Austria. URL https://www.R-project.org/ (Access confirmed on 2021. 3. 1.)

Roberts, S., Osborne, M., Ebden, M., Reece, S., Gibson, N. & Aigrain, S. (2013). Gaussian processes for time-series modelling. *Philosophical Transactions of the Royal Society A: Mathematical, Physical and Engineering Sciences 371*.

Rouse, J. W., R. H. Haas, J. A. Schell, D. W. Deering 1974. Monitoring vegetation systems in the great plains with ERTS. Proceedings of the Third Earth Resources Technology Satellite-1 Symposium; NASA SP-351. pp. 309-317.

Royle, J. A. & Link, W. A. (2006). Generalized site occupancy models allowing for false positive and false negative errors. *Ecology 87*, 835–841.

Schindelin, J., Arganda-Carreras, I., Frise, E. Kaynig, V., Longair, M., Pietzsch, T., ... & Cardona, A. (2012). Fiji: an open-source platform for biological-image analysis. *Nature methods 9*, 676-682.

Shannon, C. E. (1948). A mathematical theory of communication. *Bell System Technical Journal 27*, 379–423.

Sharif, B., Lundin, R., Morgan, P., Hall, J., Dhadda, A., Mann, C., Donoghue, D., Brownlow, E., Hill, F. Carr, G., Turley, H., Hassall, J., Atkinson, M., Jones, M., Martin, R., Rollason, S., Ibrahim, Y., Kopczynska, M. & Szakmany, T. (2016). Developing a digital data collection platform to measure the prevalence of sepsis in Wales. *Journal of the American Medical Informatics Association 23*, 1185–1189.

Sharkey, T. D. and Loreto, F. (1993). Water stress, temperature, and light effects on the capacity for isoprene emission and photosynthesis of kudzu leaves. *Oecologia 95*, 328-333.

Shell, G. S. G., Lang, A. R. G. & Sale, P. J. M. (1974). Quantitative measures of leaf

orientation and heliotropic response in sunflower, bean, pepper and cucumber. *Agricultural Meteorology 13*, 25-37.

Shigesada, N. (1992). Mathematical model for biological invasions (Up Biology 92). University of Tokyo Press, Tokyo, pp. 24-45. [in Japanese]

Shiyomi, M., Takahashi, S., Yoshimura, J., Yasuda, T., Tsutsumi, M., Tsuiki, M. & Hori, Y. (2001). Spatial heterogeneity in a grassland community: Use of power law. *Ecological Research 16*, 487-495.

Sinclair, T. R., Shiraiwa, T. and Hammer, G. L. (1992). Variation in crop radiation use efficiency with increased diffuse radiation. *Crop Science 32*, 1281-1284.

Stoll, P. & Prati, D. (2001). Intraspecific aggregation alters competitive interactions in experiment plant communities. *Ecology 82*, 319-327.

Su, Y. & Yajima, M. (2015). R2jags: Using R to Run 'JAGS'. R package version 0.5-7. https://CRAN.R-project.org/package=R2jags (Access confirmed on 2021. 3. 1.)

Susko, D. J. & Mueller, J. P. (1999). Influence of environmental factors on germination and emergence of *Pueraria lobata*. *Weed Science 47*, 585-558.

Suzuki, Y., Okamoto, H., Hirata, T., Kataoka, T. & Shibata, Y. (2010). Estimating spatial distribution of herb species and herbage mass in cover crop field using hyperspectral imaging. *Japanese Journal of Farm Work Research 45*, 99-109.

Takahashi, T. & Yasuoka, Y. (2006). Estimating leaf area index of riverine vegetation using hyperspectral remote sensing and vegetation index. *Proceedings in hydraulic engineering 50*, 1213-1218.

Tanaka, J., Horie, N. & Hayakawa, N. (2008). The test of get rid of invaded *Pueraria lobata* (Willd.) Ohwi at slope planting. *Journal of the Japanese Society of Revegetation Technology 34*, 215-218.

Tanaka, J., Horie, N. & Hayakawa, N. (2009). The test of get rid of invaded *Pueraria lobata* (Willd.) Ohwi at slope planting (II): Two years after. *Journal of the Japanese Society of Revegetation Technology 35*, 170-173.

Tanaka, J. & Yamaguchi Y. (2016). Utilization of metal plate barrier for inhibiting growth of *Pueraria lobata* (Willd.) Ohwi. *Journal of the Japanese Society of Revegetation Technology 41*, 468-471.

Tashima, R., Sakaguti, N. & Gyokusen, K. (2004). Leaf movements in Japanese black pine (*Pinus thunbergii*). *Kyushu Journal of Forest Research 57*, 215-216.

Thanyapraneedkul, J., Muramatsu, K., Daigo, M., Furumi, S., Soyama, N., Nasahara, N. K., Muraoka, H., Noda, M. H., Nagai, S., Maeda, T., Mano, M., Mizoguchi, Y., (2012). A vegetation index to estimate terrestrial gross primary production capacity for the global change observation mission-climate (GCOM-C)/second-generation global imager (SGLI) satellite sensor. *Remote Sensing 4*, 3689 - 3720.

Tietz, S., Hall, C. C., Cruz, J. A. and Kramer, D. M. (2017). $NPQ_{(T)}$: a chlorophyll fluorescence parameter for rapid estimation and imaging of non-photochemical quenching of excitons in photosystem-II-associated antenna complexes. *Plant, Cell & Environment 40*, 1243-1255.

Tsugawa, H. & Kayama, R. (1974). Studies on population structure of kudzu vine 1. On the thickening growth of internodes of stems and main roots, the number of their vascular bandle rings. *Journal of Japanese Grassland Science 20*, 181-188.

Tsugawa, H. & Kayama, R. (1975). Studies on population structure of kudzu vine 2. A method for classification and presentation of root systems. *Journal of Japanese Grassland Science 21*, 207-212.

Tsugawa, H. & Kayama, R. (1978). Studies on population structure of kudzu vine 4. The diiference in the distribution pattern of rooted nodes and of stumps classified by the developmental stage of their root system. *Journal of Japanese Grassland Science 23*, 307-311.

Tsugawa, H. & Kayama, R. (1981a). Studies on dry matter production and leaf area expansion of kudzu vines (*Pueraria lobate* Ohwi) I. The dry weight and leaf area of the current year's stem produced from the node of the overwintering stem. *Journal of Japanese Grassland Science 27*, 267-271.

Tsugawa, H. & Kayama, R. (1981b). Studies on dry matter production and leaf area expansion of kudzu vines (*Pueraria lobata* Ohwi) II. The difference in dry matter and leaf area productivity between the main stem and the branches of the current year's stem. *Journal of Japanese Grassland Science 27*, 272-276.

Tsugawa, H., Sasek, T. W., Tange, M. & Nishikawa, K. (1987). Studies on dry matter production and leaf area expansion of kudzu vines (*Pueraria lobata* Ohwi) III. The emergence of current year's stems from overwintering stems. *Journal of Japanese Grassland Science 32*, 337-347.

Tsugawa, H., Sasek, T. W., Komatsu, N., Tange, M. and Nishikawa, K. (1989). Seasonal changes in dry matter production and leaf area expansion of first year stands of kudzu-

vine (*Pueraria lobata* OHWI) differing in spacing. Journal of Japanese Grassland Science 35, 193-205.

Tsutsumi, M., Shiyomi, M., Takahashi, S. & Sugawara, K. (2001). Use of beta-binomial series in occurrence counts of plant populations in sown grasslands. Grassland Science 47, 121-127.

Vehtari, A., Gelman, A. & Gabry, J. (2017). Practical Bayesian model evaluation using leave-one-out cross validation and WAIC. *Statistics and Computing 27*, 1413-1432.

Venables, W. N. & Ripley, B. D. (2002). Modern Applied Statistics with S. Fourth Edition. Springer, New York.

Veran, S., Kleiner, K. J., Choquet, R., Collazo, J. A. & Nichols, J. D. (2012). Modeling habitat dynamics accounting for possible misclassification. *Landscape Ecology 27*, 943-956.

Vos, J., Evers, J. B., Buck-Sorlin, G. H., Andrieu, B., Chelle, M. & de Visser, P. H. B. (2010). Functional-structural plant modelling: a new versatile tool in crop science. *Journal of Experimental Botany 61*, 2101–2115.

Waite, S. (1994). Field evidence of plastic growth responses to habitat heterogeneity in the clonal herb *Ranunculus repens*. *Ecological Research 9*, 311–316.

Watanabe, O., Otani, I. & Ohara, G. (2005). Estimation of the above ground plant biomass on the paddy levees environment using the hyper-spatial image data. *Journal of the Japanese Agricultural Systems Society 21*, 47-57.

Watanabe, S., Nakano, Y. & Okano, K. (2001). Comparison of light interception and field photosynthesis between vertically and horizontally trained watermelon (*Citrullus lanatus* (Thunb.) Matsum. et Nakai) plants. *Journal of Japanese Society for Horticultural Science 70*, 669-674.

Weaver, M. A., Boyette, C. D. & Hoagland, R. E. (2016). Rapid kudzu eradication and switchgrass establishment through herbicide, bioherbicide and integrated programmes. *Biocontrol Science and Technology 26*, 640-650.

Wien, H. C. & Wallace, D. H. (1973). Light-Induced Leaflet Orientation in *Phaseolus vulgaris* L. *Crop Science 13*, 721-724.

Woebbecke, D. M., Meyer, G. E., Von Bargen, K. & Mortensen, D. A. (1995). Color indices for weed identification under various soil, residue, and lighting conditions.

Transactions of the American Society of Agricultural Engineers 38, 259-269.

Xu, F., Guo, W., Wang, R., Xu, W., Du, N. & Wang, Y. (2009). Leaf movement and photosynthetic plasticity of black locust (*Robinia Pseudoacacia*) alleviate stress under different light and water conditions. *Acta Physiologiae Plantarum 31*, 553-563.

Yamamoto, Y., Wakabayashi, D., Saji, K., Kodani, T., Iwamoto, H. and Yamada, H. (2018). Guard fence for vines. Japan patent P2018-105122A. [in Japanese]

Yamori, W., Makino, A. & Shikanai, T. (2019). A physiological role of cyclic electron transport around photosystem I in sustaining photosynthesis under fluctuating light in rice. *Scientific Reports 6*, 20147.

Yasuda, T., Shiyomi, M. & Takahashi, S. (2003). Differences in spatial heterogeneity at the species and community levels in semi-natural grasslands under different grazing intensities. Grassland Science 49. 101-108.

Zhang, R. & Shea, K. (2012). Integrating multiple disturbance aspects: management of an invasive thistle, *Carduus nutans*. *Annals of Botany 110*, 1395-1401.

Zhang, R. & Shea, K. (2019). Working smarter, not harder: objective-dependent management of an invasive thistle, *Carduus nutans*. *Invasive Plant Science and Management 12*, 155-160.

Zheng, Y., Zhu, Q., Huang, M., Guo, Y. & Qin, J. (2017). Maize and weed classification using color indices with support vector data description in outdoor fields. *Computers and Electronics in Agriculture 141*, 215-222.

Publication list

(Peer-reviewed articles)

Iwamoto, H. and Watanabe, O. 2020. Detection and spatial occupancy evaluation of kudzu community based on supervised classification of UAV imagery. *Journal of Weed Science and Technology* 65, 95-102.

Iwamoto, H. and Watanabe, O. 2021. Estimation of leaf area index based on spectral reflectance and its application to the evaluation of the spatial distribution of a kudzu-dominated community. *Journal of Weed Science and Technology* 66 (under printing).

(Oral presentation)

Iwamoto, H. and Watanabe, O. 2018. Detection of kudzu canopy and the evaluation of abundance by processing of aerial image. 57th Conference of Weed Science Society of Japan.

Iwamoto, H. and Watanabe, O. 2018. Attempt to detect community of kudzu and to evaluate its abundance by high-resolution aerial image processing. 65th Conference of Remote Sensing Society of Japan.

Iwamoto, H. and Watanabe, O. 2019. Detection of *Pueraria lobata* community by aerial image processing and evaluation of abundance with vegetation index. 58th Conference of Weed Science Society of Japan.

Iwamoto, H. and Watanabe, O. 2019. Sequential evaluation of spread of kudzu community by aerial image processing. 27th Asian-Pacific Weed Science Society Conference.

Iwamoto, H. and Watanabe, O. 2020. Evaluation of *Pueraria lobata* community behavior by aerial image processing and dynamic site occupancy model. 59th Conference of Weed Science Society of Japan.

Abstract

Kudzu (*Pueraria lobata* (Willd.) Ohwi) has caused economic and ecological problems in agriculture and vegetation management. Monitoring and modeling of such invasive weed community dynamics on a management scale can provide practical knowledge for optimal resource allocation to prevent its expansion. Aerial imagery obtained by unmanned aerial vehicles (UAVs) enables us to monitor the spatial distribution of a weed community. To extract information about a particular species from high-resolution sequential images, classification by machine learning should be suitable. In addition, the parameters measured by handheld chlorophyll fluorescence sensors are appropriate to analyze the photosynthetic functions of a weed community in the field. In this study, I investigated the ecological traits and optimal management of the kudzu community with novel sensing technologies.

The transition of the kudzu community's spatial distribution was investigated based on sequential UAV images. The images were divided into grids (50 × 50 cm), and each grid was classified into one of two classes (presence/absence of kudzu) based on the brightness of RGB images by support vector machine (SVM). The classifiers, which were trained by 5% of all grids, achieved an accuracy of over 0.9 and an F-measure of greater than 0.9 after the coverage of canopy in July, whereas the occupancy was not successfully classified in June. The margin of the community expanded quickly during the period of leaf expansion (July). During the period of accumulation (August–October), photosynthetic products accumulated in the storage organs, and the community expanded in the area in which kudzu was mowed at the end of July. In addition, multiple regression models were used to estimate the leaf area index (LAI) from three vegetation indices from June to August (adjusted $R^2 = 0.421–0.570$). The LAIs estimated by the regression models were found to decline in the center of the kudzu community from July to August, as clusters of high LAI values moved from the center to the outer margins of the community. This change might be attributed to the spread of leaves on higher-order branches that occurs in the renewal process of leaves during summer. The translocation of leaves from the center to the margin of a community was thought to contribute to the photosynthetic efficiency of the canopy and community expansion.

To evaluate the spatial dynamics of the kudzu community in each period, the

occupancy states of each grid were applied to a hidden Markov model (HMM). The model comprised the classification process and transition of the occupancy state. The parameters on emergence and expansion were inferred by the Markov chain Monte Carlo (MCMC) method. The posterior distribution of the parameters indicated that the expansion rates after mowing in July were relatively higher than those in August. The spatial occupancy dynamics indicated that the shoots that emerged from the residual overwintering stems and the crown roots grew quickly and compensated for the damage. For containment of the kudzu community, it will be effective to prevent rooting and accumulation of photosynthetic products into storage organs by removing higher-order branches, especially at the margin of the community in midsummer.

Furthermore, I examined the effect of leaf orientation on radiation interception and the photosynthetic efficiency of the kudzu canopy using a portable fluorometer. The leaf movement at the canopy's surface was restrained using a nylon net. The light intensity and the photosynthetic parameters of each layer were measured using a fluorometer. Paraheliotropic movements helped the uppermost leaves avoid intense direct solar radiation and increased light penetration into the canopy. The linear electron flow in the lower leaves increased while that at the surface did not decrease considerably from the light-saturated values, suggesting that the photosynthetic efficiency of the canopy as a whole improved by light penetration. The lower leaves exposed to intense light dissipated excess energy with non-photochemical quenching. Therefore, the adaptive function of leaf orientation seemed to maximize the photosynthetic efficiency of the canopy while avoiding photoinhibition in individual leaves on the surface.

These novel methods contributed to revealing important traits of the spatial dynamics and photosynthetic function of the kudzu community in the field. The sensing and modeling in this study can be extended to other weed species. Aerial image processing technology, including machine learning, is valuable to evaluate the spatial distribution of a particular weed species. Flexible hierarchical models should be developed to incorporate several kinds of sensing data for an inclusive understanding of ecological traits. Compilation of knowledge on ecological traits and framework of data processing would enable us to simulate weed community dynamics on a management scale.

Acknowledgments

I acknowledge with gratitude the big debts that I owe to many people for their contributions to this thesis.

I appreciate Dr. Osamu Watanabe for his discerning support and patience during this study. I am indebted to all the members of the Laboratory of Crop Science and Weed Science of Shinshu University.

I acknowledge the precise and suggestive advice of Dr. Taisuke Yasuda (Mount Fuji Research Institute) and Dr. Kenji Takizawa (National Institute for Basic Biology). I am also grateful to Dr. Aki Mizuguchi (Fukui Prefectural University) and her students for allowing me to participate in their project and conduct their lecture.

Appendix

Appendix 1: The JAGS script of the model in Chapter 3

```
model {

  ## observation model
  for(t in 1:T) {
    for(i in 1:I) {
      O[i, t] ~ dbern(p.tp[t] * z[i, t] + p.fp[t] * (1 - z[i, t]))
    }
  }

  ## initial distribution and system model
  for(i in 1:I) {
    z[i, 1] ~ dbern(z.zero[i] + gamma[i, 1] * (1 - z.zero[i]))
    for(j in 1:J) {
      g[i, j, 1] <- z.zero[j] * ind1[i, j] * ind2[i, j] * exp(- a[1] * r[i, j])
    }
    for(t in 2:T) {
      z[i, t] ~ dbern(z[i, t-1] + gamma[i, t] * (1 - z[i, t-1]))
      for(j in 1:J) {
        g[i, j, t] <- z[j, t-1] * ind1[i, j] * ind2[i, j] * exp(- a[t] * r[i, j])
      }
    }
    for(t in 1:T) {
      gamma[i, t] <- 1 - (1 - e[t]) * prod(f[i, , t])
      for(j in 1:J) {
        f[i, j, t] <- 1 - g[i, j, t]
      }
    }
  }
```

```
    ## prior distribution
    for(t in 1:T) {
        p.tp[t] ~ dbeta(1, 1)
        p.fp[t] ~ dbeta(1, 1)
        e[t] ~ dbeta(1, 1)
        a[t] ~ dunif(0, 10)
        Dhalfpd[t] <- log(0.5) * (-1) / (a[t] * days[t])
    }

}
```

Appendix 2: The R script for calculation in MCMC method in Chapter 3

```
# input data
class <- read.csv(file='class.csv', header = TRUE)
grid <- read.csv(file='grid.csv', header = TRUE)
days <- read.csv(file='days.csv', header = TRUE)
n.i <- nrow(grid)
n.t <- nrow(days)
o <- matrix(class$o, nrow = n.i, ncol = n.t)
rownames(o) <- 1:n.i
colnames(o) <- 1:n.t
z.zero <- grid$z.zero
x <- grid$x # x[i]: x origin of grid i in Japanese Plane Rectangular Coordinate System VIII
y <- grid$y # y[i]: y origin of grid i in Japanese Plane Rectangular Coordinate System VIII
r <- matrix(0, nrow = n.i, ncol = n.i)
ind1 <- matrix(0, nrow = n.i, ncol = n.i)
ind2 <- matrix(0, nrow = n.i, ncol = n.i)
for (i in 1:n.i) {
   for (j in 1:n.i) {
      r[i, j] <- sqrt((x[i] - x[j])^2 + (y[i] - y[j])^2)
      ind1[i, j] <- ifelse(r[i, j] > 0, 1, 0)
      ind2[i, j] <- ifelse(r[i, j] <= 3, 1, 0)
   }
}
days <- days$days
data.list <- list(I = n.i,
                  J = n.i,
                  T = n.t,
                  o = o,
                  z.zero = z.zero,
                  r = r,
                  ind1 = ind1,
                  ind2 = ind2,
```

```
                    days = days)

# initial values
inits <- list(p.tp = rep(0.5, n.t),
              p.fp = rep(0.5, n.t),
              e = rep(0.5, n.t),
              a= rep(1, n.t))
inits.list <- list(inits, inits, inits)
inits.list[[1]]$.RNG.name <- "base::Mersenne-Twister"
inits.list[[1]]$.RNG.seed <- 123
inits.list[[2]]$.RNG.name <- "base::Mersenne-Twister"
inits.list[[2]]$.RNG.seed <- 123
inits.list[[3]]$.RNG.name <- "base::Mersenne-Twister"
inits.list[[3]]$.RNG.seed <- 123

# MCMC sampling
library(runjags)
result <- run.jags(method = "parallel",
                   model = "model.txt",
                   monitor = c("deviance", "p.tp", "p.fp", "e", "a", "Dhalfpd"),
                   data = data.list,
                   inits = inits.list,
                   n.chains = 3,
                   adapt = 100,
                   burnin = 100,
                   sample = 1000,
                   thin = 5)

# output result
write.table(summary(result), "result.csv", sep = ",")
codaSamples <- as.mcmc.list(result)
library(R2jags)
traceplot(codaSamples)
```